Characterization of a pre-curved needle for use in Distal Tip Manipulation Mechanism

by

Jeremy Contini Franklin

SUBMITTED TO THE DEPARTMENT OF MECHANICAL ENGINEERING IN PARTIAL FULFILLMENT OF THE REQUIREMENTS FOR THE DEGREE OF

BACHELOR OF SCIENCE
AT THE
MASSACHUSETTS INSTITUTE OF TECHNOLOGY

JUNE 2009

Signature of Author: _____
Department of Mechanical Engineering
May 17, 2009

Certified by: _____
Alexander H. Slocum
: of Mechanical Engineering
Thesis Supervisor

Accepted by: _____
John H. Lienhard V
Professor of Mechanical Engineering
Chairman, Undergraduate Thesis Committee

Characterization of a pre-curved needle for use in Distal Tip Manipulation Mechanism

by

Jeremy Contini Franklin

Submitted to the Department of Mechanical Engineering
on May 18, 2009 in partial fulfillment of the
requirements for the Degree of Bachelor of Science in
Mechanical Engineering

ABSTRACT

The knowledge and technical expertise required for the development of telerobotic systems capable of needle distal tip manipulation is the focus of this thesis. An extensive prior literature review was conducted to examine (1) the current medical devices available to pulmonary radiologists and (2) the current steerable mechanism state of the art. Interviews were also conducted with interventional radiology and cardiology physicians at the Massachusetts General Hospital to define the mechanism functional requirements for a telerobotic system and a first order analysis was undertaken to evaluate three strategies.

The selected strategy was based on the concept of deploying a flexible pre-curved stylet from a concentric straight cannula. Analytical models were developed to (1) understand what material properties are required to recover from the imposed strains, (2) compare stylet stiffness relative to each other and the cannulas, and (3) calculate the deployment and retraction forces required for moving the stylet relative to the cannula. Sixteen Nitinol stylets were prototyped and experiments were performed with four different diameter cannulas and an experimental setup and methodology was developed to measure the deployment and retraction forces. The data collected for 48 permutations of stylet diameter, stylet bend radius, and cannula gauge were compared to the analytical model.

Retraction forces were measured between .277 and 13.9N, and deployment forces were measured between .191 and 6.95N. For a given cannula it was found that force increases as stylet diameter increases and bend radius decreases. The analytical model better matched the experimental retraction and deployment measurements for the smaller stylet diameters (0.508 and 0.635 mm) with low friction, retraction and deployment forces. It was found that the retraction and deployment force does not necessarily increase or decrease with cannula diameter and it was found that the stylets drawn through the 16 gauge cannula consistently had the lowest deployment and retraction forces recorded across the four cannulas tested. Ultimately, the experimental and analytical tools developed in this thesis helped us select appropriate needle materials and mechanism components for use in a telerobotic system that is under development.

Thesis Supervisor: Alexander H Slocum
Title: Professor of Mechanical Engineering

Acknowledgements

I would like to thank Professor Slocum for providing me with the opportunity to do research with such supportive graduate students during the final year of my undergraduate education. The design processes I learned researching in PERG will help me immensely in the years to come.

I would like to thank Conor Walsh for his guidance, support and mentoring during the research and writing of this thesis. Also, thanks to Nevan Hanumara and Brett van Zuiden for generously volunteering product design and analysis assistance.

Special thanks to my parents, Nora and John, my sister, Emma, my aunts and uncles, Barbara, Pat, John and Janice, and my cousins, Justin and Lena for your endless support, love and encouragement. I would not be here without you.

Table of Contents

List of Figures

List of Tables

Chapter 1: Introduction

In many areas of medical treatment today, noninvasive treatments are replacing traditional surgeries because of their decreased cost, decreased risk to the patient, and decrease in patient recovery time. Percutaneous procedures – inserting needles and probes through a single puncture of the skin – have increased in number and effectiveness with the use of medical imaging technologies such as Computed Tomography (CT), Ultrasound, and Fluoroscopy. During procedures like lung and liver biopsies, needles must be quite long (10-20 cm) to extend deep into a patient's body. In recent years, researchers have improved the accuracy of these procedures by coupling the high resolution imaging information to the precision of a robotic device [1]. These systems offer the potential to reduce the overall procedure time and radiation dose to the patient while offering more effective diagnosis and treatment for the patient.

Typically, robotic systems that have been developed operate by orienting the needle about a fixed point at the skin surface before inserting it to a precise depth. However, this approach means that the distal tip of the needle cannot be precisely repositioned after it has been inserted into the body. Conversations with Rajiv Gupta, MD and Jo-Anne Shepard, MD of Massachusetts General Hospital revealed that such a capability of precise *distal tip manipulation* would benefit the diagnosis and treatment of pulmonary lesions within the lung's complex and fragile interior. Specifically, a steerable system could help doctors treat patients faster with fewer needle insertions and for some patients potentially replace traditional open-chest surgery with a non-invasive alternative.

To begin development of this device, an extensive prior literature review was conducted to learn what mechanisms have already been developed for steering the distal tips of medical instruments. It was found that there are several families of products used in the lung, spine, brain, and cardiovascular system that are used in hospitals today. However, all these products are manually operated, thus requiring direct manipulation and positioning by the hands of a surgeon.

The goal of our group is to develop a telerobotic system that is capable of accurately steering remotely the distal tip of needles that are typically used for percutaneous applications. In an effort to support the ultimate development of this system, this thesis

focuses on: (a) a prior literature review of existing steerable medical devices; (b) the selection of one mechanism, (c) analytical and (d) experimental characterization of the forces necessary for the operation of such a mechanism across a range of critical dimensions. To better characterize the behavior and performance of this type of needle tip steering mechanism, empirical and analytical models of: (1) Deployment/Retraction Forces, (2) Cutting Forces, and (3) Needle Point Accuracy were made. This thesis begins the characterization by focusing on analytically and experimentally determining the deployment and retraction forces.

Chapter 2: Prior Literature Review

Before developing a mechanical system that contacts points in a control volume, an extensive prior literature review was conducted to examine (1) the current medical devices available to pulmonary radiologists and (2) the current steerable mechanism state of the art.

Current Percutaneous Needle Systems Used in the Lung

Radiologists today use handheld devices to diagnose and treat pulmonary lesions (lung cancer) in patients. To diagnose lung cancer, a tissue sample is percutaneously taken from the patient using a *biopsy needle*. Aspirating biopsy needles, like the Cook Medical Chiba® Needle shown below, sample tissue by inserting a cannula containing a concentric solid stylet into the body at a position determined by medical imaging. Radiologists use CT-scans and careful, manual adjustments to position the needle correctly in the lung. After insertion, the solid, central stylet is removed, allowing radiologists to aspirate tissue into the hollow center of the cannula. More aggressive tissue sampling is performed with *coring biopsy needles* like the Cook Medical Quick-Core® Biopsy Needle shown below. The device is deployed in the same manner as standard biopsy needles, guided into the patient with CT scans.

After diagnosis, tumors are treated in a number of invasive or noninvasive procedures. *Radio Frequency Ablation* (RFA) is one treatment technique that is becoming increasingly popular among radiologists because of its effectiveness and minimal invasiveness. RFA probes, like the Valleylab Cool-tip™ RF units shown below, are deployed with the same CT-guided procedure as biopsy needles. Once inserted into a tumor, an RFA probe uses high frequency alternating current to burn the cancerous tissue surrounding it. A single RFA probe produces a cylindrical burn volume around its distal tip between .8 and 4.2cm in diameter [2].

Currently, the procedures radiologists use to perform biopsies and RFA procedures have a number of limitations. The thin medical instruments have a tendency to deflect and deviate from their desired trajectory and also there are areas within the body where it is difficult to position a needle effectively. In the lung, blood vessels and bronchia block

areas of the organ for treatment with needles and probes. Radiologists also struggle to burn large tumors using RFA. For large or oblong-shaped tumors, Radiologists use multi-tip RFA probes to treat the lesion, puncturing the lung at multiple points and causing trauma to good tissue as it cuts through the organ towards its target lesion. Large RFA probes also can burn significant volumes of healthy tissue during treatment.

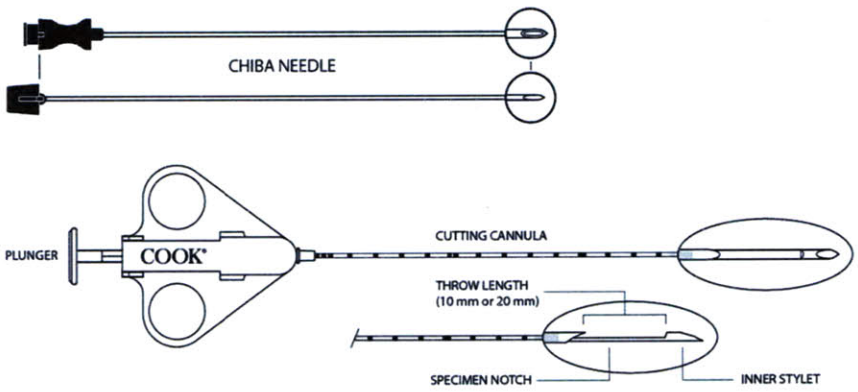

Figure 3.1: Cook Medical CHIBA® Hollow Cannula and Solid Stylet (top) and Quick-Core® (bottom) biopsy needles. [3]

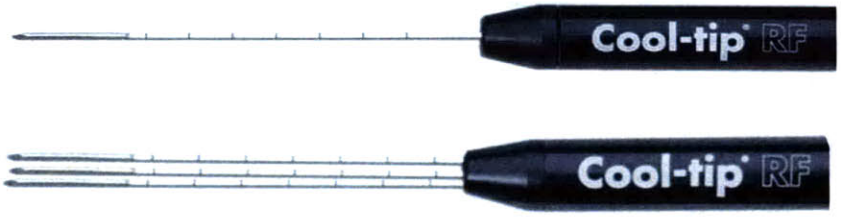

Figure 3.2: Valleylab Cool-tip™ RF single and triple-prong probes. [4]

Patent & Prior Literature Review for Steerable Mechanisms in Medical Devices

A prior literature survey of medical devices was conducted to identify steerable mechanisms and strategies that have already been developed. The literature search was conducted by searching for journal articles on Google Scholar (http://scholar.google.com) and searching for patents and patent applications on Free Patents Online (www.freepatentsonline.com).

Two forms of steerable medical devices were found in the prior literature review: steerable catheters and steerable needles. While both are capable of distal tip steering, as

catheters pass through channels within the body they are designed to steer in free space or fluid-filled conduits. Steerable needles, on the other hand, are designed to maneuver through tissue. To alter direction, steerable elements must be pre-curved when retracted and deployed along a curved path into tissue or an organ or else use the reaction forces at the tip of the needle for steering.

Steerable Catheters

Many steerable medical device patents identified pertain to catheter design. Catheters are tubes that can be inserted into vessels, arteries, and ducts in the body. Catheters pass through so many convoluted channels in the body, including portions of cardiovascular system and urinary tract that there have been many mechanisms designed for this application. The catheter designs found are manipulated by changing the angles of joints or weak sections along the length of the catheter. These mechanisms are shown in greater detail in Mechanisms 1-5 of Appendix 1. These catheters typically are capable of steering in a body cavity and do not lend them selves to steering in tissue. Catheter steering mechanisms are highly flexible to effectively maneuver through the body, but the mechanisms studied can reorient the system direction through external deformation of part of the system. In an environment like the lung where a device must cut through tissue, large external motions are difficult to do in an accurate way and will result in undesirable damage to healthy tissue.

Steerable Needles

Several patents were also found on methods for steering within tissue. Mechanisms No. 5 & 6 in Appendix 1 highlight ways of steering within tissue using concentric pre-bent needles and "airfoil" needle shapes. These designs make use of specialized cutting surfaces to direct the orientation of the medical device. Mechanisms 7 & 8 show two strategies for changing the orientation and curvature of tissue harvesting and surgical devices in free space.

Mechanisms 9-11 in Appendix 1 show devices that use concentric compliant cylinders to change the orientation of the tip of a needle. Distal tip manipulation is achieved with a variety of strategies: bending the cannula with a pre-bent stylet, deploying a pre-bent stylet from a straight rigid cannula, and bending a stylet with a

feature in the cannula lumen. Of all the mechanisms reviewed, Mechanisms 9-11 have applications that are most closely related to the functional requirements and design parameters driving the design of our system.

Current Commercial Generation of Steerable Needles

Samples of three steerable needles in use on the market today, the COOK Pakter Curved Needle Set, the COOK Osteo-Site Bone Access Products, and the PneumRx Seeker Biopsy Needle were also examined. The Pakter and Osteo-Site products both employ pre-bent needles in concentric rigid cannulas. The Pakter and Osteo-Site products implement distal-tip needle steering to access the center of damaged vertebrae and spinal disks. The Seeker needle, on the other hand bends its cannula into its target shape by a cable driven stylet controlled by a joystick.

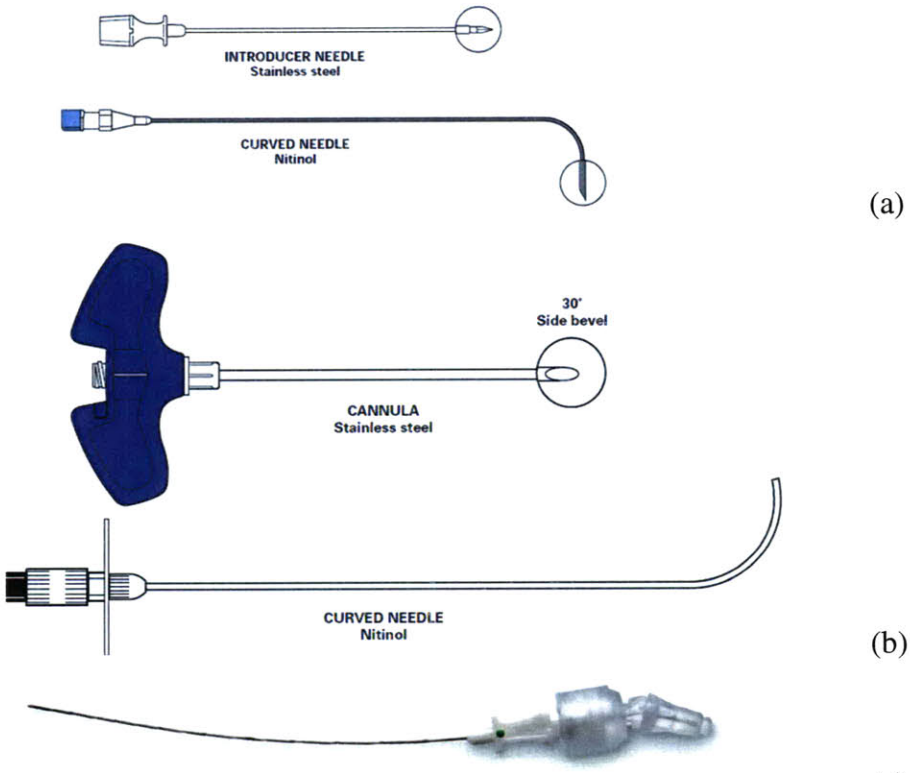

Figure 3.3: Cook Medical Pakter® Needle [5](a); Cook Medical Osteo-Site® [6](b); PneumRx Seeker® Biopsy Needle [7](c)

Chapter 3: Mechanism Selection

With a more complete understanding of the current technology and procedures used in image-guided percutaneous lung procedures today, additional interviews were conducted with surgeons in Interventional Radiology and Cardiology at Massachusetts General Hospital to define the critical areas of study and the functional requirements that will dictate mechanism selection for a telerobotic system.

Problem Definition and Functional Requirements

It was decided that the first step in producing a viable robotic steerable needle is to develop an analytical and experimental understanding of the forces and mechanisms required to accurately target any point within a control volume of an organ or in tissue.

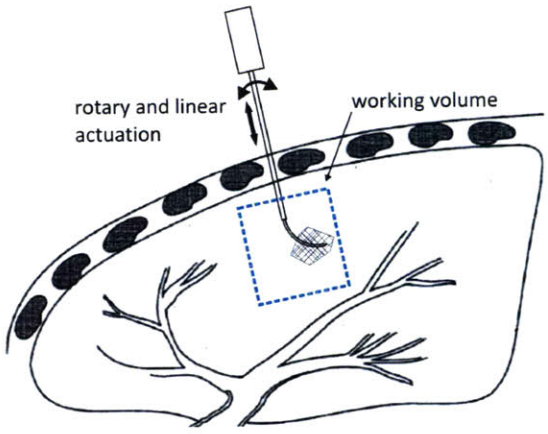

Figure 3.1: Potential embodiment of needle with distal tip manipulation operating within the lung.

A list of critical functional requirements and corresponding design parameters based on medical requirements set by Dr. Gupta, and engineering requirements set by Conor J. Walsh and Jeremy Franklin. The numerical specifications listed in Table 3.1 are approximate values based on an initial assessment of radiologist needs in an assistive system.

Table 3.1: Functional Requirements & Design Parameters of Steerable Needle

Functional Requirements	Design Parameters	Design Parameter Specifications
1. Compactness	Mechanism is deployed through a needle into the lung.	Maximum $D_{Needle} = 2.1$mm Minimum $D_{Mechanism} \approx .7$mm

		(R. Gupta) & [8]
2. Can cut through tissue	Maintains desired insertion direction while cutting through tissue.	Satisfies accuracy criteria for $F_{tissue\ cut}$ = 5-8N (C.J. Walsh)
3. Workspace	Can contact any point in a cylindrical work volume of pulmonary tissue.	$h_{cyl} = D_{cyl}$ = 5cm (R. Gupta)
4. Degrees of Freedom	Needle requires 3 Degrees of Freedom	Contacts any point within the workspace (C.J. Walsh & J. Franklin)
5. Precision & Reliability of Motion	System must contact same point as predicted by kinematic model.	Tip position within ±1mm of calculated position. (C.J. Walsh)
6. Ease of Manipulation	System must be easy to operate using a small, patient mounted robot.	Maximum needle deployment or retraction F_{Max} < 30N (C.J. Walsh & J. Franklin)
7. CT-Scan Compatibility	Presence of instrument does not adversely affect functionality of CT imager.	No metal components can cross the central axis of the needle. (C.J. Walsh)

Each of the steerable needle mechanisms found on the market today and in the prior literature search was examined and assessed as to whether each design strategy could be applied to meet the functional requirements and design parameters. Particular attention was given to Functional Requirements 2 and 3 and assessing whether each mechanism could steer in homogenous and inhomogeneous tissue. Overall, three main distal tip needle manipulation strategies were identified from the prior literature review and commercially available products:

Table 3.2: Summary of Prior Literature Review Findings

Strategy	Mechanisms Found in Review
1. Actuation of flexible segments of a device in free space	Mechanisms 1-4, 7 & 8, Appendix 1; Seeker Biopsy Needle.
2. Using reaction forces of the material that the device is passing through to alter the device trajectory	Mechanisms 5 & 6, Appendix 1.
3. Using concentric compliant mechanisms to change device orientation	Mechanisms 9-11, Appendix 1; Pakter Needle; Osteo-Site Rx.

From Strategies 1 & 3, three preliminary mechanism embodiments were developed and assessed to see whether they could fulfill the design parameters. Embodiments pertaining to strategy 2 were not explored further because controlled steering requires knowledge of the material properties which would vary at different points in the body as well as between patients. Thus, given the porous, inhomogeneous structure of pulmonary tissue, it was decided that Strategy 2 did not meet Functional Requirement 3, and would be difficult to implement in the lung. Next, the validity of each mechanism was assessed using first order analysis to see if there is any material or geometric limitations that would discourage further development of any design.

The three potential embodiments are:

I. *Cable-Actuated Needle in Straight Cannula:* From Strategy 1. Deploying a steerable, cable driven needle, like the Seeker Biopsy needle, through a concentric outer cannula to achieve distal-tip steering. The three degrees of freedom are (1) translation of cannula relative to patient, (2) translation of cable-actuated needle relative to cannula and (3) shortening of needle cables to vary the radius of curvature with which the inner needle deploys.

II. *Cannula-Directed Needle Steering:* From Strategy 3. Using a feature or mechanism at the distal end of a straight cannula to change the direction of a straight stylet passing through it. The three degrees of freedom are (1) rotation of the cannula, (2) translation of the straight stylet relative to the cannula and (3) rotation of the cannula.

III. *Pre-Bent Needle in Straight Cannula:* From Strategy 3. Like the Pakter needle, this strategy employs a constant radius pre-bent needle deployed through a concentric outer cannula. The three degrees of freedom are (1) translation of the cannula, (2) translation of the straight stylet relative to the cannula and (3) rotation of the cannula.

Decision to Pursue Embodiment III

After assessing all three embodiments, Embodiment III was chosen for its simple mechanical design and strategy that has been validated by the commercialized of the Pakter and Osteo-Site needles. Strain and Geometry analysis of Embodiments I and II also suggested that they would be limited in system rigidity relative to Embodiment III for the size of needles that were considered.

To evaluate Embodiment II, $\varepsilon_{max} = \frac{R}{\rho}$ (1) was used to show that the minimum bend radius that a .7mm diameter Nitinol stylet can withstand without yielding is a 5.7mm. A 5.7mm bend radius feature could be included in the cannula described in Embodiment II, but the deployment angle would be limited compared to a pre-bent stylet, and it was decided that that prototyping a cannula with such a small, high precision feature was beyond the scope, budget, and timeline of this project.

Bench level testing showed significant promise for Embodiments I & II. Ultimately, the cable-actuated strategy was ruled out because a pre-bent needle was judged to be mechanically simpler with fewer modes of failure. Additionally, an examination of the cross-sectional area of a needle with cables running axially down its length showed that significant internal space within a cable driven needle was allocated to the control system. For pre-bent needles contained within a 14G cannula, the needle diameter can be increased to a 17G or 18G needle (17G OD = 1.47mm). A 22G RFA probe [8], can be deployed through a 14G needle surrounded by a ring of control cables. A comparison of cross sectional areas, however, suggests there is benefit to deploying a larger diameter stylet for improved stiffness capability. Table 4.1 shows that increasing the diameter of the needle dramatically increases the stiffness of the system (moment of area is proportional to diameter to the fourth power). An 18G pre-bent needle has area moment of inertia of $1.3*10^{-13}m^4$, 10 times greater than the area moment of a 22G needle. Having the area to increase the diameter of the inner needle allows designers to increase the rigidity of the steerable stylet, reducing the magnitude of deflections caused by tangential and off-axis loading and cutting through tissue.

While observing the Seeker Biopsy needle, additional questions were raised about the robustness of Embodiment I. Walsh & Franklin struggled to manually position the Seeker accurately with the product's joy stick. Because the system is so flexible, they found it difficult to produce exactly the same bend geometry and orientation. From these observations, it was concluded that compliance in the cables and steering mechanisms must be characterized before further development is done with this embodiment to determine if Seeker's design ultimately limits the accuracy of a distal tip manipulation system. Due to time constraints, these tests were not designed or carried out, and Embodiment 3 was selected for its simplicity and rigidity as shown in Table 3.3.

Table 3.3: Embodiments 1-3 Mechanism Selection Pugh Chart

	Embodiment I	**Embodiment II (Normalized)**	**Embodiment III**
Stiffness	0	0	(+)
Low Number of Components	(–)	0	0
Manufacturability	0	0	(+)
Total	**-1**	**0**	**2**

Material Selection

Before prototyping a pre-bent needle system, a set of material criteria were defined for the bent stylet:

1. Stylet must not undergo plastic deformation during its deployment from or retraction into the cannula. $\left(\varepsilon_{stylet-Max} < \varepsilon_{strain}\right)$
2. Material must be biocompatible: qualified and safe for use in medical devices in the body.
3. Material must be commercially available for prototyping.
4. Material must come in wire form to aid prototyping.

Nitinol and stainless steel (www.fwmetals.com) wire were chosen as initial candidates. Nitinol exhibits two material properties depending on its alloy, superelasticity and shape memory, which are used extensively in medical devices. Both properties come from Nitinol's ability to transition between different phases, between Austenite and

Martensite, when placed under high stress or temperature. In the steerable needles, Nitinol's superelasticity needs to be well understood to produce precise curves in the sample wire and utilize the flexibility of the material.

Superelastic Nitinol can withstand strains of up to 6-10% with little to no yielding in conditions around the alloy's Active Austenite Finishing Temperature. [9] At high stress, austenitic Nitinol is induced into a deformed martensitic crystal structure, allowing it to elongate with relatively constant stress applied to it. Nitinol is not stable at this temperature in its martensitic state, and will revert to austenite when the stress is relieved. The result is a metal with remarkable strain recovery properties. Material property data from this project's Nitinol and stainless steel supplier, Fort Wayne Metals, helped characterize the expected performance of Nitinol and compare it to stainless steel.

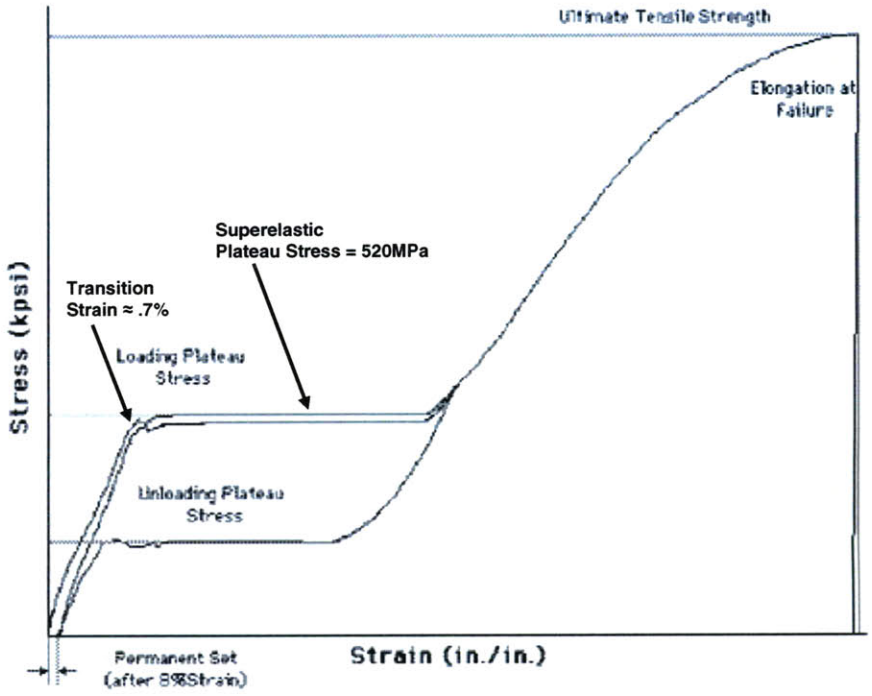

Figure 3.2: Stress vs. Strain Tensile Test Curve for Nitinol [9]

The transition strain of Nitinol – the strain required to initiate a phase transformation within Nitinol – was calculated to better predict Nitinol's behavior in an analytical model. The transition strain was calculated using the Young's modulus in Table 3.4, and the assumption was made that the loading plateau stress remains constant at 517MPa for the entire plateau:

$$E_{NiTi-Specified} = 75GPa$$

$$\sigma_{plateau-Specified} = 517MPa$$

$$\varepsilon_{Trainsition} = \frac{\sigma_{plateau-Specified}}{E_{NiTi-Specified}} = .7\%$$

The material properties listed in Table 3.4 and extrapolated from Figure 3.2 were used in conjunction with a strain analysis to compare how Nitinol and stainless steel will perform when retracted into a cannula.

Table 3.4: Summary of Material Properties used for Material Selection Analysis [9] [10]

Material Property	Nitinol	Stainless Steel
Young's Modulus	75GPa	193GPa
Yield Strength (.2% Yield)	N/A	205MPa
Loading Plateau Stress (4% Strain)	517 MPa	N/A
Unloading Plateau Stress (4% Strain)	241 MPa	N/A
Elastic/Superelastic Transition Strain	.7%	N/A
Permanent Set (after 6% Strain)	0.25%	N/A
Permanent Set (after 8% Strain)	0.50%	N/A
Ultimate Tensile Strength	>1310 MPa	515MPa
Elongation Failure (after heat treatment)	>11%	N/A

Both Nitinol and stainless steel satisfy material selection criteria 2-4 listed above. However, as will be discussed in Chapter 4, strain analysis of wire bending suggests that stainless steel will yield during deployment and retraction tests. Therefore, Nitinol was chosen for the pre-bent stylet material.

Chapter 4: Analysis

In this chapter the analysis used to (1) understand what material properties are required to recover from the imposed strains, (2) compare stylet stiffness, and (3) calculate the deployment and retraction forces required to push and pull a pre-bent stylet through a straight cannula is outlined.

Strain Calculations & Analysis

Simple strain calculations were conducted to determine the approximate longitudinal strains expected for straightening the pre-bent stylets as they are retracted into their outer cannulas across the range of target volumes being investigated. Using the maximum strain for a straight rod bent to a radius of curvature was calculated using $\varepsilon_{\max} = \frac{d/2}{\rho}$ (1), where ρ = needle bend radius. Equation (1) assumes a linear stress distribution which is a reasonable assumption for all the cases analyzed as the bend radii are all large (>10 times) relative to the wire radii [11]. The results are plotted in Figure 4.1.

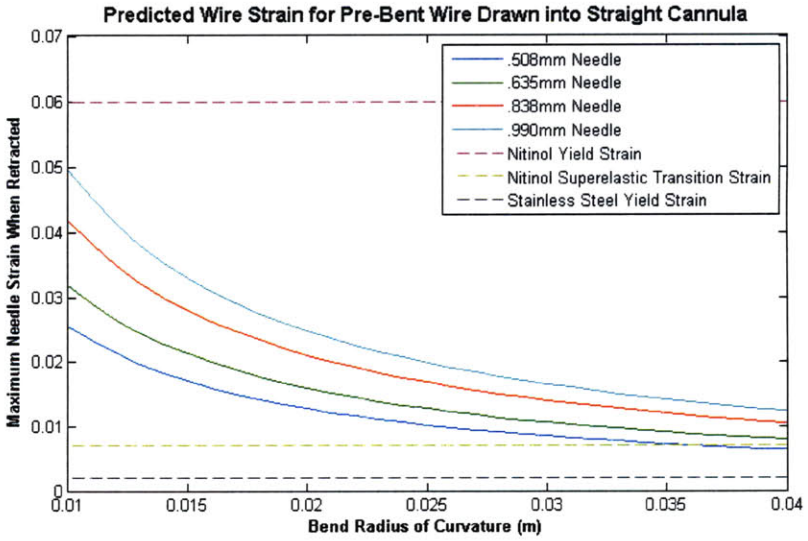

Figure 4.1: Predicted Wire Strain for Pre-Bent Wire Drawn into Straight Cannula. Note: Diameters .508mm, .635mm, .838mm, and .990mm were chosen for analysis due to their commercial availability.

Figure 4.1 suggests that for Nitinol, the vast majority of stylets having bend radii in the range of 10mm-40mm are strained in the superelastic region, but are not expected to undergo plastic deformation. Further, it also shows that stainless steel, while appropriate

for use in many medical devices, is unsuited for this application. Extrapolations of Nitinol Yield Strain (6%) and Nitinol Superelastic Transition Strain (.7%) were shown in Chapter 3. The Stainless Steel Yield Strain value of (.2%) was assumed from standard steel stress-strain tables. [10]

Concentric Needle Area Moment of Intertia Comparison

The area moment of inertia of a single hollow 14 gauge cannula and the four stylet diameters were calculated and are compared in Table 4.1. The equations for calculating the second area moment of inertia are as follows:

$$I_{circle} = \frac{\pi d^4}{64}$$
$$I_{tube} = \frac{\pi d_{outer}^{\ 4}}{64} - \frac{\pi d_{inner}^{\ 4}}{64} \qquad (2)$$

Table 4.1: Comparison of Area Moments of Inertia of a hollow cannula and solid stylets.

	14 Gauge (Hollow)	18 Gauge	20 Gauge	22 Gauge	24 Gauge
Area Moment of Inertia (m^4)	6.51E-13	1.28E-13	3.34E-14	1.30E-14	5.04E-15
Fraction of AMoI of 14 Gauge Hollow	1	1.96E-01	5.12E-02	2.00E-02	7.74E-03

It was found that the 14G cannula has an area moment of inertia 10-100 times great than stylets that can fit in it. Additionally, Table 4.1 shows that an 18G needle has roughly ten times the area moment of inertia as a 22G needle. While there are 20 and 22G RFA probes available, it may be to the advantage of a pre-bent steerable system to use a larger gauge probe that is stiffer, and will therefore deflect less from off-axis loading as it cuts through tissue.

Retraction & Deployment Force Calculations

A. Overall Modeling Strategy

To calculate the retraction force of a pre-bent needle being drawn into a cannula, the stress distribution within the superelastic wire was first characterized, a neutral axis was determined, and energy methods were used to derive the force required to unbend a

curved needle. Under high tensile strain, Nitinol deforms along a superelastic plateau (Figure 3.2). To model this material nonlinearity, Nitinol was modeled as an elastic-perfectly plastic material and composite beam theory was used to find an effective stiffness to be applied in energy methods.

B. Assumptions

Several critical assumptions were made in developing an analytical model of this system.

1. Nitinol acts as a linear elastic material in compression. In tension, it is modeled as linear elastic up to its superelastic threshold stress of σ_{SE}, at which point it is modeled as having a Young's modulus of zero along the superelastic plateau (see Figure 3.2).
2. In its superelastic transition phase, Nitinol experiences a constant stress of σ_{SE} =517MPa.
3. The ratio of bend radius to wire diameter is very large (always >10). This assumption allows for modeling the stress distribution within the stylet as linear and with a correction factor k.

C. Finding Neutral Axis

To find the Neutral Axis of the stylet, the position along the cross section where the internal stress is zero, the stylet is modeled as a curved cylinder of radius ρ. The wire is treated as a composite beam with A_{SE} loaded with a constant stress of 517MPa, and areas A_1 and A_2 undergoing elastic deformation with the stress distribution of a curved beam in pure bending:

$$\sigma_z = -Ek\frac{R-y}{y} \qquad (3)$$
$$\rho \le y \le \rho + d$$

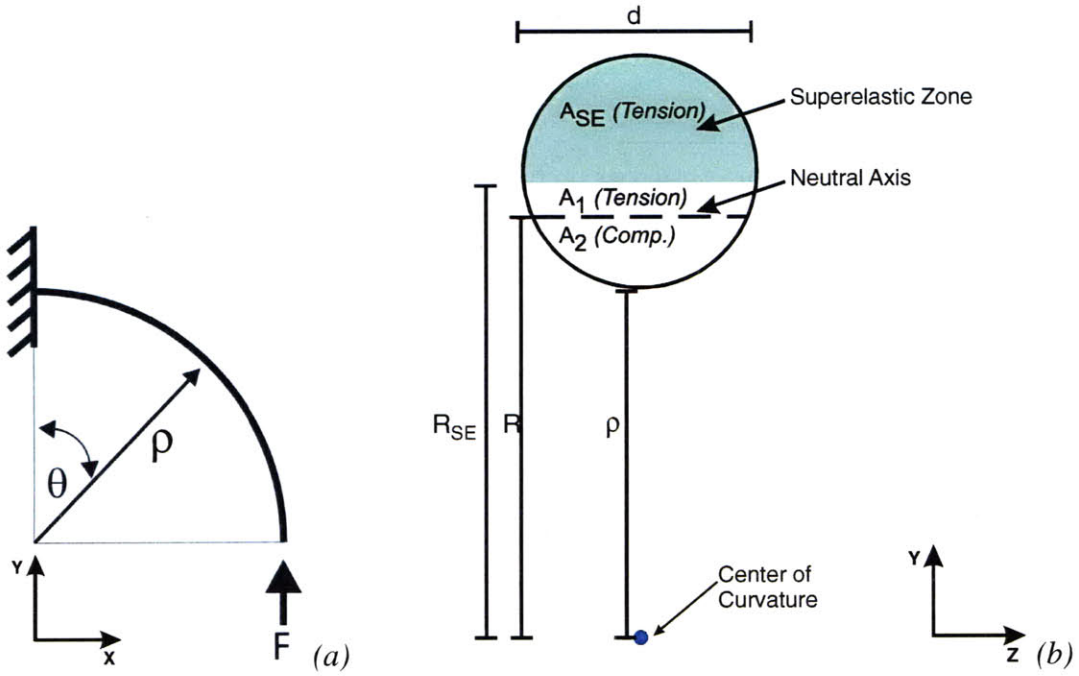

Figure 4.2: (a) Side view of analytical wire model and (b) Cross Sectional view of bending superelastic wire. Figures not to scale.

Using the principle of static equilibrium, and assuming that the stresses due to bending dominate, the net axial in the wire can be equated to zero:

$$0 = \int_{A_{SE}} \sigma_{SE} dA + \int_{A_1+A_2} \sigma_E dA \tag{4}$$

$$0 = \int_{A_{SE}} \sigma_{SE} dA + \int_{A_1+A_2} Ek\left(\frac{R-\rho}{\rho}\right) dA \tag{5}$$

In Equations (4) and(5), σ_{SE} is the wire's superelastic plateau stress (517MPa), σ_E is the stress distribution experienced by the linear elastic portion of the beam. E is the Young's modulus for small strains of Nitinol (75MPa). In Equation(5), k is approximated as k=1.1 because the ratio of bend radius to wire diameter is greater than 10. [12] A relation between R_{SE} and R is identified based on the superelastic transition stress σ_{SE} in a curved beam with elastic stress distribution.

$$\sigma_{SE} = Ek\frac{R-R_{SE}}{R_{SE}}$$
$$R_{SE} = \frac{REk}{(\sigma_{se}+Ek)} \tag{6}$$

Solving Equation (5) numerically in Maple (www.maplesoft.com), R is found for a given d and ρ:

$$\int_{\rho}^{R_{SE}} \sigma_{SE} 2\sqrt{\left(\frac{d}{2}\right)^2 + \left(y-\rho-\frac{d}{2}\right)^2}\,dy + \int_{\rho}^{R_{SE}} \frac{2Ek(R-y)}{y}\sqrt{\left(\frac{d}{2}\right)^2 + \left(y-\rho-\frac{d}{2}\right)^2}\,dy = 0 \qquad (7)$$

D. Finding Effective Stiffness

With values for R, composite beam bending theory is applied to find an effective stiffness, EI_{eff}, for a beam that has a partially elastic, partially plastic (superelastic) stress distribution. Modeling the elastic region of the wire with Young's Modulus E, and the plastic (superelastic) region with a Young's modulus of 0, EI_{eff} can be obtained from:

$$\begin{aligned} EI_{eff} &= \int_{A} E(y)y^2 dA \\ EI_{eff} &= \int_{A_{SE}} 0 \mathrm{g} y^2 dA + \int_{A_1+A_2} E(y)y^2 dA \\ EI_{eff} &= \int_{A_1+A_2} E(y)y^2 dA \end{aligned} \qquad (8)$$

This integral expands to:

$$EI_{eff} = \int_{-\frac{d}{2}+(R_{SE}-\rho)}^{\frac{d}{2}} 2Ey^2\sqrt{\left(\frac{d}{2}\right)^2 - y^2}\,dy \qquad (9)$$

In Equation (9), the effective stiffness at the structure's maximum strain state is evaluated, i.e. for a straight beam bent to the initial radius of curvature of the stylet. It should be noted that for a few cases, the maximum strain in the wire was calculated to be less than the 0.7% transition strain and so the beam was consider as purely elastic and Equation (9) was not used.

E. Finding Force (F)

To determine the force F shown in Figure 4.2, linear elastic energy methods are applied for curved beam geometry. The energy contained within the curved beam shown in Figure 4.2 is:

$$U = \frac{1}{2}\int_0^{\pi/2} \frac{M^2 \rho}{EI} d\theta \qquad (10)$$

The bending moment M is expressed as:

$$M = F\rho\cos\theta \qquad (11)$$

In evaluating this Equation (10) two additional assumptions are made. The expression EI is approximated as EI_{eff} evaluated in Equation (9). Substituting EI with this single value assumes a constant EI based on geometric and material properties. For an elastic-perfectly plastic (superelastic) beam, however, EI_{eff} is also dependent on bend radius as shown in Equation (9). The effective stiffness of a wire bent to radius ρ was chosen as a reasonable value for the analytical model because it represents the stylet stiffness where the moment exerted on the stylet is at its greatest. Future analytical models could include an equation of EI_{eff} as a function of θ for greater accuracy.

The stress distribution model (Equation (3)) used in this analysis is based on pure moment bending. Equation (11) introduces the force F into the model. Axial loading from force F was not included in the static equilibrium analysis used to find neutral axis R. Future analytical models could include static equilibrium analysis that included a distal tip force F on a curved beam.

Substituting EI_{eff} and M into the equation and integrating along the length of the curved beam, i.e. from 0 to θ:

$$U = \frac{1}{2}\int_0^{\theta} \frac{F^2\rho^2\cos^2(\theta)\rho}{EI_{eff}} d\theta$$
$$U = \frac{F^2\rho^3}{EI_{eff}}\left[\frac{\theta}{2} + \frac{1}{4}\sin(2\theta)\right] \qquad (12)$$

The deflection due to Force F can be expressed as:

$$\delta = \rho\sin(\theta) = \frac{\partial U}{\partial F} \qquad (13)$$

Evaluating $\frac{\partial U}{\partial F}$ and solving for F yields:

$$F = \frac{EI_{eff}\sin(\theta)}{R^2\left[\frac{\theta}{2}+\frac{1}{4}\sin(2\theta)\right]} \tag{14}$$

The evaluation of $\frac{\partial U}{\partial F}$ will be much more complex if functions of EI_{eff} and R are developed based on based stylet deflection. Because energy methods are path-dependent, a more accurate model could be developed gained by modeling and the changing stress distribution within the stylet more thoroughly.

F. Finding Friction Force

Knowing force F, contact friction between the cannula and the bent stylet can be calculated. Using the assumption that, in a cannula, a bending force and its corresponding normal force equal in magnitude to F are applied and supported at two points within the cannula (Figure 4.3), the internal friction force can be characterized as follows:

$$F_{friction} = \mu F + \mu F_{nv} = 2\mu F$$
$$F_{friction} = 2\mu \frac{EI_{eff}\sin(\theta)}{R^2\left[\frac{\theta}{2}+\frac{1}{4}\sin(2\theta)\right]} \tag{15}$$

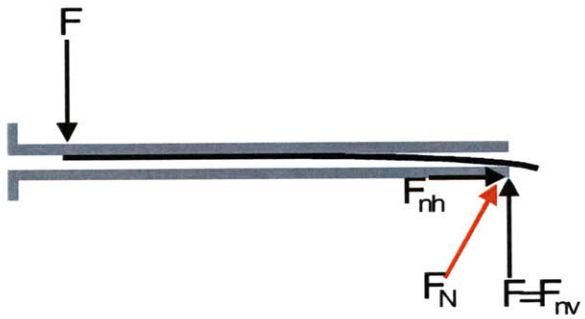

Figure 4.3: Bending and Normal force positioning in Cannula.

G. Finding Horizontal Component of Unbending Force

As shown in Figure 4.4, the stylet enters the cannula an incident angle, and therefore, a horizontal and vertical component of retraction force is expected. To calculate the full retraction force required to draw a needle into the cannula, F_{nh} is calculated to sum with the friction force. To find F_{nh}, the angle of the normal force F_N is found with the

assumption that the wire maintains its radius of curvature between the outer edge of the cannula and the cannula's upper wall as shown in Figure 4.4.

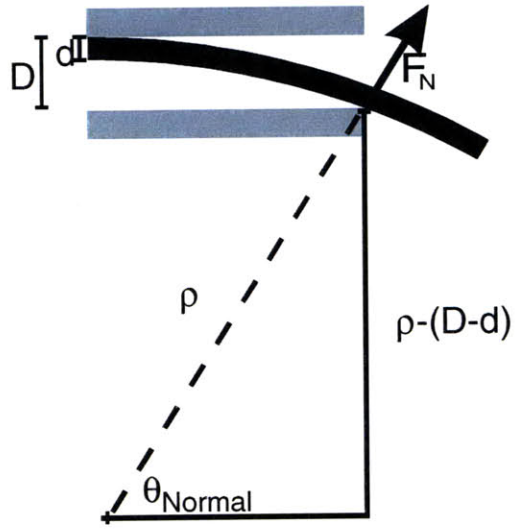

Figure 4.4: Determining angle of F_N of a curved wire passing over the corner of a horizontal cannula.

From the geometry shown in Figure 4.4, the following relationship for θ_{Normal} can be made.

$$\rho\sin(\theta_{Normal}) = \rho - \pi(D-d)$$
$$\theta_{Normal} = \arcsin\left(1-\frac{D-d}{\rho}\right) \qquad (16)$$

With F_{nv} and θ_{Normal} known, F_N, F_{nh} can be found:

$$\frac{F_{nv}}{F_{nh}} = \tan(\theta_{Normal})$$
$$F_{nh} = \frac{F_{nv}}{\tan(\theta_{Normal})} = \frac{EI_{eff}\sin(\theta)}{R^2\left[\frac{\theta}{2}+\frac{1}{4}\sin(2\theta)\right]\tan\left(\arcsin\left(1-\frac{D-d}{\rho}\right)\right)} \qquad (17)$$

H. Finding Total Retraction Force

The total retraction force can estimated as the sum of friction force $F_{friction}$ and horizontal retraction force F_{nh}:

$$F_{retract} = -F_{friction} - F_{nh}$$

$$F_{retract} = -2\mu \frac{EI_{eff}\sin(\theta)}{R^2\left[\frac{\theta}{2} + \frac{1}{4}\sin(2\theta)\right]} - \frac{EI_{eff}\sin(\theta)}{R^2\left[\frac{\theta}{2} + \frac{1}{4}\sin(2\theta)\right]\tan\left(\arcsin\left(1 - \frac{D-d}{\rho}\right)\right)} \quad (18)$$

I. Finding Deployment Force

The maximum deployment force is assumed to be the maximum friction force when the stylet has been fully retracted into the cannula (θ = 90°). Evaluating, $F_{friction}$ for θ = 90°:

$$F_{deploy} = -F_{friction}$$

$$F_{friction} = 2\mu \frac{EI_{eff}\sin(\theta)}{R^2\left[\frac{\theta}{2} + \frac{1}{4}\sin(2\theta)\right]}, \theta = \pi/2 \quad (19)$$

$$F_{deploy} = \frac{8\mu EI_{eff}}{\pi R^2}$$

The analytical models of $F_{retract}$ and F_{deploy} were compared to the results of the experiments described in Chapter 5. Plots of these comparisons are shown in the Chapter 6, and a discussion of the similarities and differences between them are discussed in Chapter 7.

Chapter 5: Experimental Methods

Experiments were performed to determine the required forces for relative motion between a cannula and a pre-bent stylet and are compared to the analytical model. To achieve this, a fixture and procedure were developed for manufacturing Nitinol stylets with varying wire diameter and bend radius. An experimental rig was then developed that enabled these stylets to be deployed from and withdrawn into a subset of Stainless Steel cannulas of various diameters.

Manufacturing Nitinol Stylets

A bend in a piece of Nitinol wire may be achieved through plastic deformation or through a heat treating process. Heat treatment was chosen for these stylets to maintain homogenous material composition throughout the stylet and avoid the residual stresses caused by cold working. The process for heat setting Nitinol has been previously reported [13] and involves evenly heating the material to an annealing temperature of 550°C where it is maintained for 3 to 15 minutes until internal stresses have been relieved, followed by a quenching operation to maintain the material in the desired Austenitic Phase (A_f). [14] Using this approach a fixture was designed that could maintain the Nitinol in its final desired shape through heating and quenching while providing minimal thermal resistance to ensure rapid quenching. Three versions of fixtures were designed and built to heat and quench Nitinol. The final design, shown in Figure 5.1, reliably manufactured pre-bent stylets that passed visual inspection tests. The components shown in Figure 5.1 have the following functions:

1. *Outline Plate:* Holds straight wire in a curved shape.
2. *Upper & Lower Vent Plates:* Holds bent wire in the plane of the Outline Plate. Allows water to pass through during quench.
3. *Wire Locating Plate:* clamps to the straight portions of the pre-bent stylets, locating them with respect to the rest of the fixture.
4. *Upper & Lower Picture Frames:* Keeps the Upper and Lower Vent Plates from bowing outward from the Outline Plate during the thermal shock of a water quench. St. Venant's principle was applied while designing the picture frames.

The primary bars are 2.5–4X the thickness of the bar to maximize exposed quench area, while minimizing rig deformation.

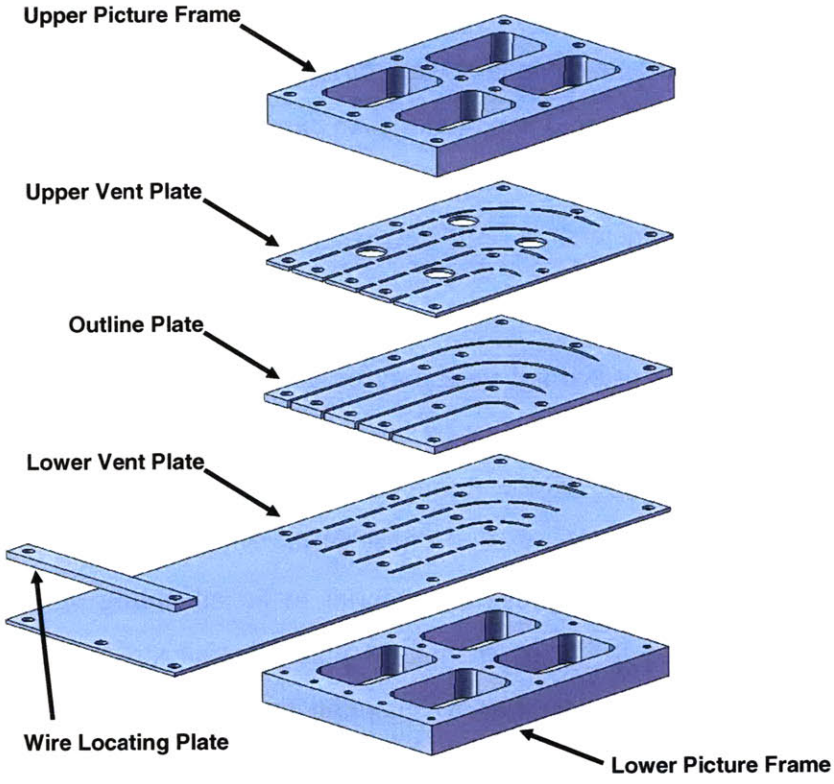

Figure 5.1: Nitinol Quench Fixture

The fixture is screwed together with 15 screws and is made out of steel to maintain its shape and strength at 550C. After building a functional rig, a procedure was developed and followed for producing all 16 pre-bent stylets. See Appendix 2 for descriptions and images earlier fixture versions.

Procedure for Manufacturing Pre-Bent Nitinol Needles

The procedure for manufacturing pre-bent stylets began with preparing straight annealed superelastic Nitinol for quenching. Four pieces of each diameter wire being tested were cut to 1'8" lengths and a 30° point was ground into one end. To grind the wires, each was inserted through a cannula so its tip was exposed at the other end. The wire was angled 15° off the face of diamond grinding wheel for carbide machine tools, pushed the distal end of the wire against the wheel. The wire was also rotated so as to produce a symmetric conical tip.

With sharpened tips at the end of each stylet, sets of four wires were placed in the Nitinol Quench Fixture. The lower half of the fixture (Lower Picture Frame, Lower Vent Plate, and Outline Plate) was pinned together with screws, and then each wire was placed into the four channels on the Outline Plate. To keep the wires located during assembly, each wire was taped to the fixture with scotch tape. The upper half of the fixture (Upper Vent Plate, Upper Picture Frame) was then screwed on with a drill gun. Finally, the straight ends of the wires were located in place with the Wire Locating Clamp.

An annealing oven (www.lindbergmph.com) was then pre-heated to 550C, and a 5-gallon water bucket was filled with tap water (Water Temperature = 20-25C). When the furnace reached 550C, the assembled fixture was placed in the furnace and a 15 minute timer was started when the oven returned to 550C. After 15 minutes, the fixture was removed with heavy tongs and dunked into the bucket of water while stirring vigorously. Moments after quenching, the fixture was cool enough to touch, and it was disassembled, the finished stylets were removed, the water was replaced, and four new straight wires with a different diameter were put in the furnace for the same heat treatment.

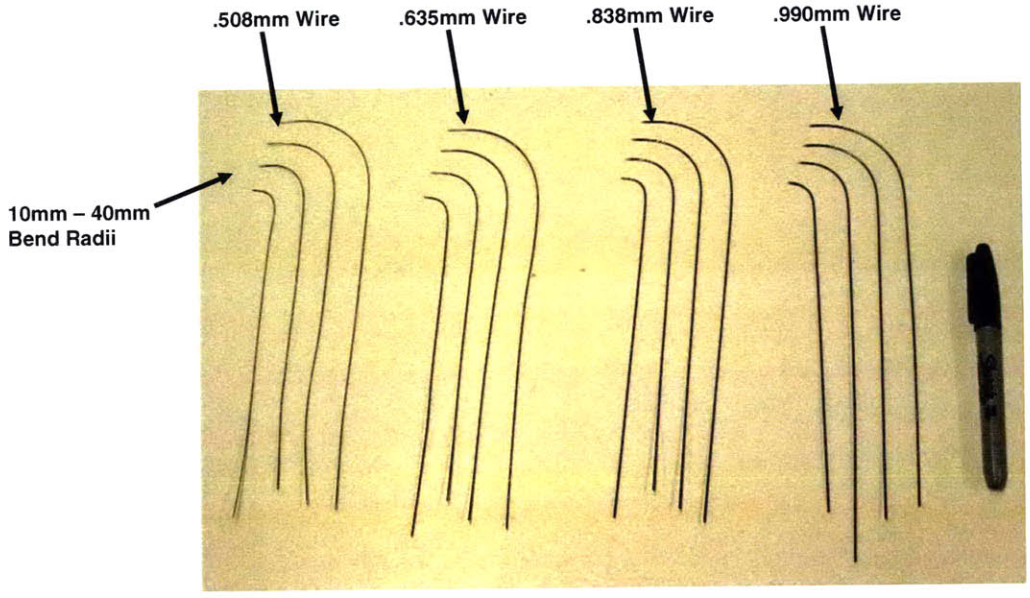

Figure 5.2: Pre-bent Nitinol Needles manufactured with the heat treatment process described above.

Retraction & Deployment Force Experiment Materials

The following materials & equipment are used to conduct the Retraction & Deployment Force Experiment:

1. ADMET eXpert 560QP Universal Testing Machine (www.admet.com)
2. MTESTQuattro ADMET control software (www.admet.com)
3. Windows PC that meets the system requirements of the ADMET software package. (www.Dell.com)
4. 2.2lbf Interface Force Transducer (www.interfaceforce.com)
5. Needle Testing Fixture
6. Cannulas: (4X) Cannulas with flat smooth tips. (14G, 16G, 18G, 20G) (Figure 5.4)
7. Needles: (16X) Pre-Bent Needles. Four sets of needles are needed (Diameters .508mm, .635mm, .838mm, .990mm) with each needle in each set having different bend radius (10mm, 20mm, 30mm, 40mm) (Figure 5.2)

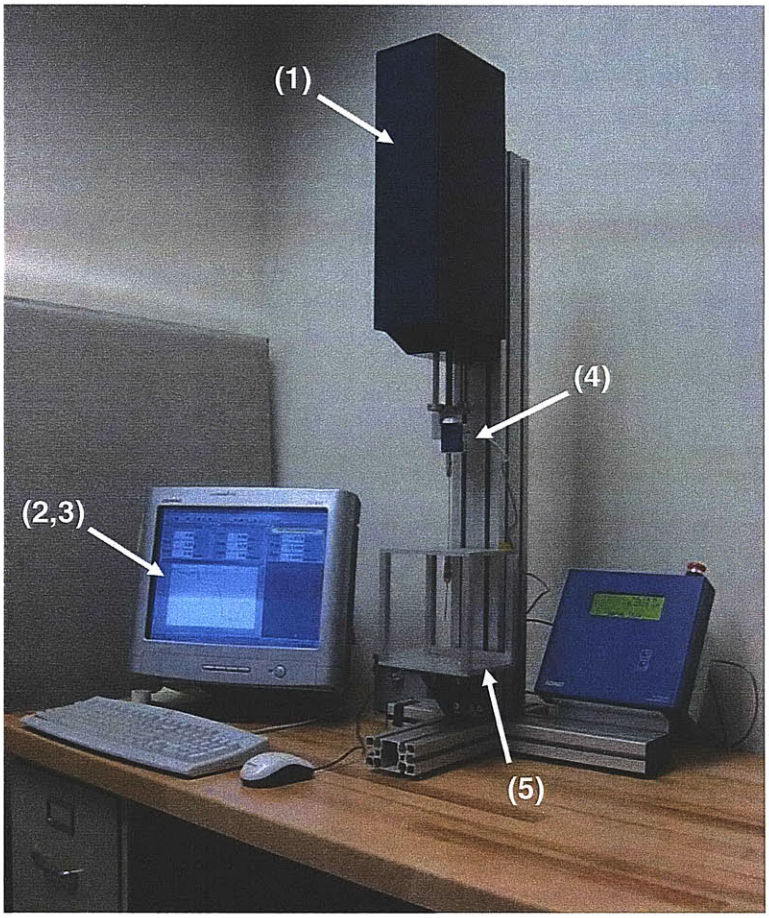

Figure 5.3: Needle Testing Fixture mounted in a PC-Controlled ADMET 5601QP Universal Testing Machine.

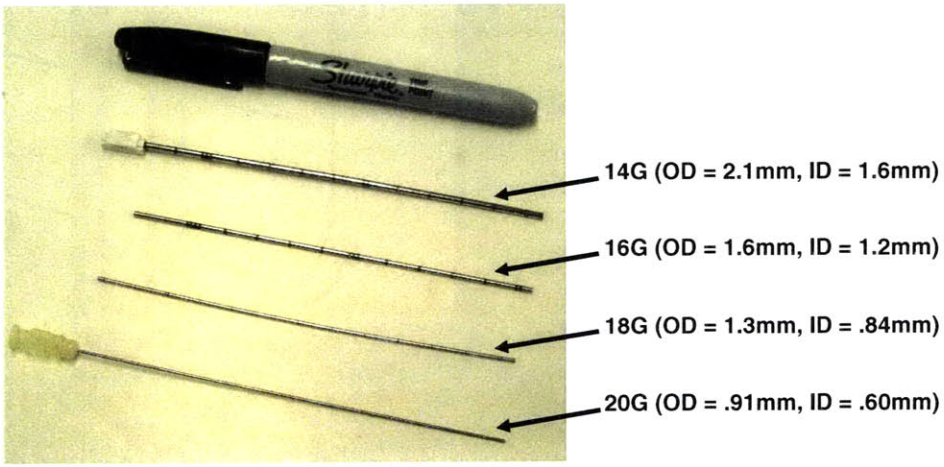

Figure 5.4: 20G, 18G, 16G, 14G flat-tipped cannulas for deployment and retraction tests.

Four standard cannulas were provided by Dr. Rajiv Gupta to be modified for the deployment and retraction tests. Each cannula was cut down to 11cm in length, and any burs from the cut were professionally removed with a metal buffing tool. For experimentation, the cannulas were mounted in a custom-made needle testing fixture shown in Figure 5.5. The fixture was designed to (1) bolt to the ADMET universal testing machine, (2) hold a cannula rigidly and vertically, and (3) provide enough space for ballistics gel samples to be held under a cannula. The fixture screwed into the ADMET using the standard 40mm square hole pattern on its base. It held a cannula at it center with a pin vice (www.mcmaster.com). A matching pin vice screwed into the load cell above the test fixture to hold the stylet.

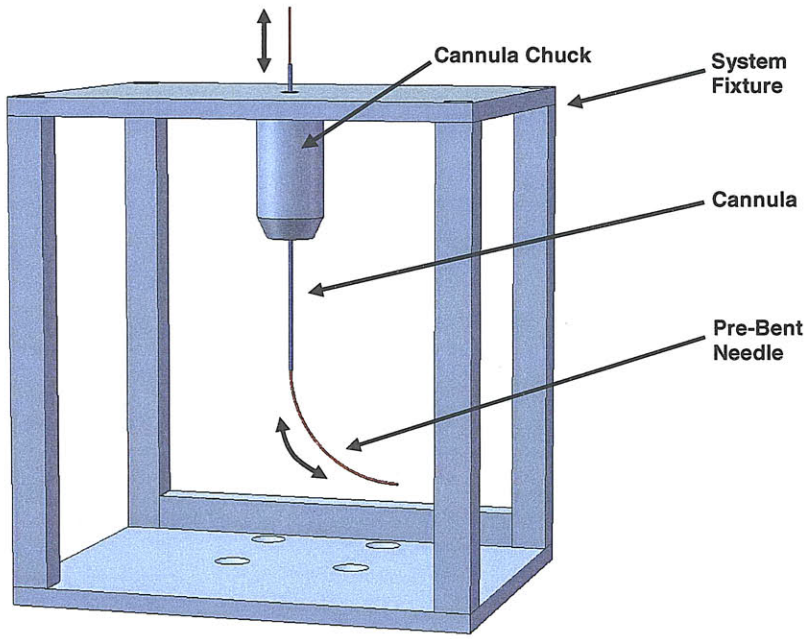

Figure 5.5: Needle Testing Fixture

Retraction & Deployment Force Experiment Procedure

Data were recorded for 48 permutations of cannula diameter, wire diameter, and bend radius to identify trends across all three dimensions. At the beginning of each test, the Needle Testing Fixture was fastened to the ADMET machine, the PC was set to record data and deploy the stylet at 7.5mm/sec, a cannula was flushed with Isopropyl alcohol and attached to the Needle Testing Fixture to let dry, and a stylet was cleaned by the experimenter with Kimwipes and Isopropyl alcohol.

Each stylet was positioned within the test cannula such that the tip of the stylet was drawn approximately 10mm inside the cannula. Before running the ADMET, the operator marked the position of the cannula and stylet relative to their pin vices to monitor slipping between the stylet and pin vice. Each stylet was deployed and retracted 5 times through the cannula, with force measurements from each run stored on the PC hard drive.

Data Recording & Analysis

After each sequence of five runs, the data sets were imported into Microsoft Excel and force measurements were normalized about the deployment/retraction transition

point. Plots were made of the average max deployment and retraction measurements found in each set of five runs, with error bars expressing the standard deviation found between the five runs. Some cannula/stylet/bend radius combinations were not run because (1) the retraction forces exerted fell outside of the load capacity of the 2.2lb load cell, (2) some stylets with small bend radii could not be inserted into the smallest diameter cannula.

Chapter 6: Results

Data was collected and analyzed for 48 combinations of stylet diameter, stylet bend radius, and cannula gauge. The full results of the experimental and analytical models are tabulated and plotted in Appendix 3. Retraction forces were measured between 0.277 and 13.9N, and deployment forces were measured between 0.19 and 6.95N. The standard deviations between runs of the same stylet and cannula were calculated to be 2-19% for retraction forces and 1-10% for deployment forces.

Test Run Characterization

During each deployment/retraction test, several loading regimes were observed and characterized and a representative plot for .508mm stylet, 14 gauge cannula and 30mm bed radius is shown below in Figure 6.1.

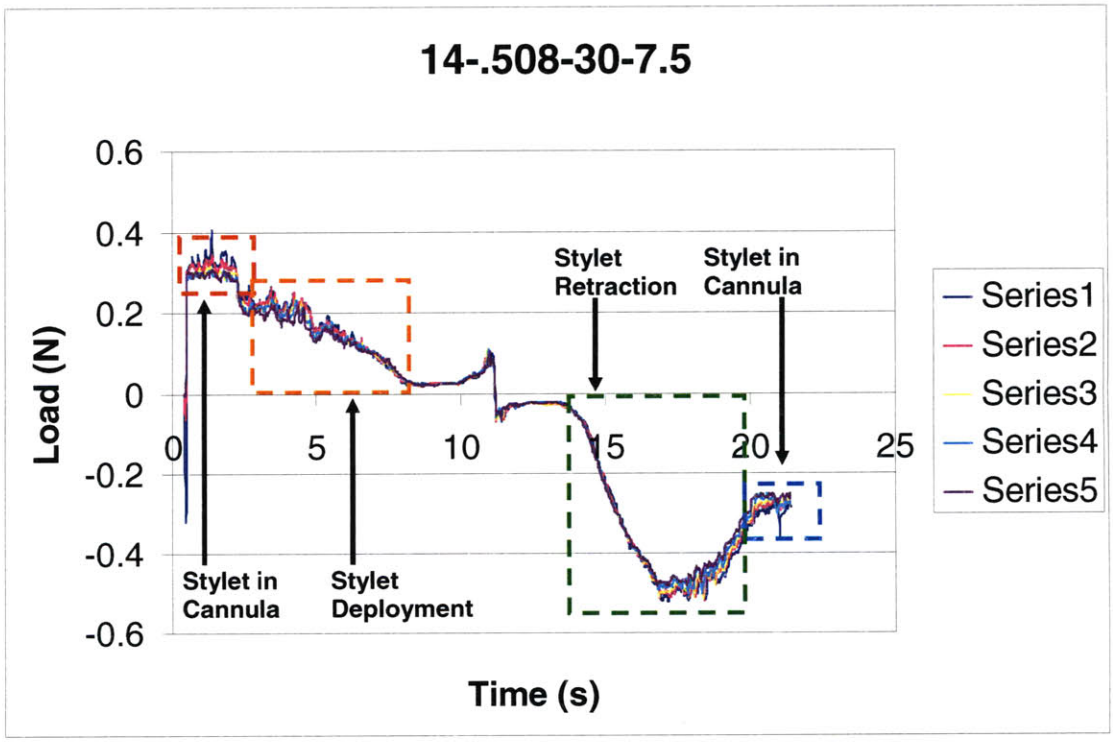

Figure 6.1: Load vs. Time plot for 5 runs of .508mm stylet with 30mm bend deployed through a 14G cannula at 7.5mm/sec

Starting from the left of the time axis, relative motion between the stylet and cannula when the stylet was completely within the cannula produced a nearly constant force as

measured with the load cell. As the stylet was deployed from the cannula the force was observed to decrease until it reached a level close to zero when the curved portion of the stylet was completely deployed. Some small force was still observed due to slight misalignment between the cannula and stylet. The direction of movement of the ADMET machine was then reversed and hence the sign of the force changes. Retraction of the stylet into the cannula resulted in an increasing force that reached a peak and then reduced to a steady state value that was of a similar value to that observed just before the stylet was deployed from the cannula as we would expect.

Test Run Observations

While recording individual deployment/retraction tests, several unexpected observations were made during several experimental runs. Figure 6.1, for example, shows a steep increase in deployment force at the end of its stroke, right before changing directions and beginning its retraction. Additionally, larger than normal standard deviations between force measurements were calculated for several runs. Figure 6.2 illustrates one such example where the deployment force increases between successive runs, with the retraction force also changing but with less variation.

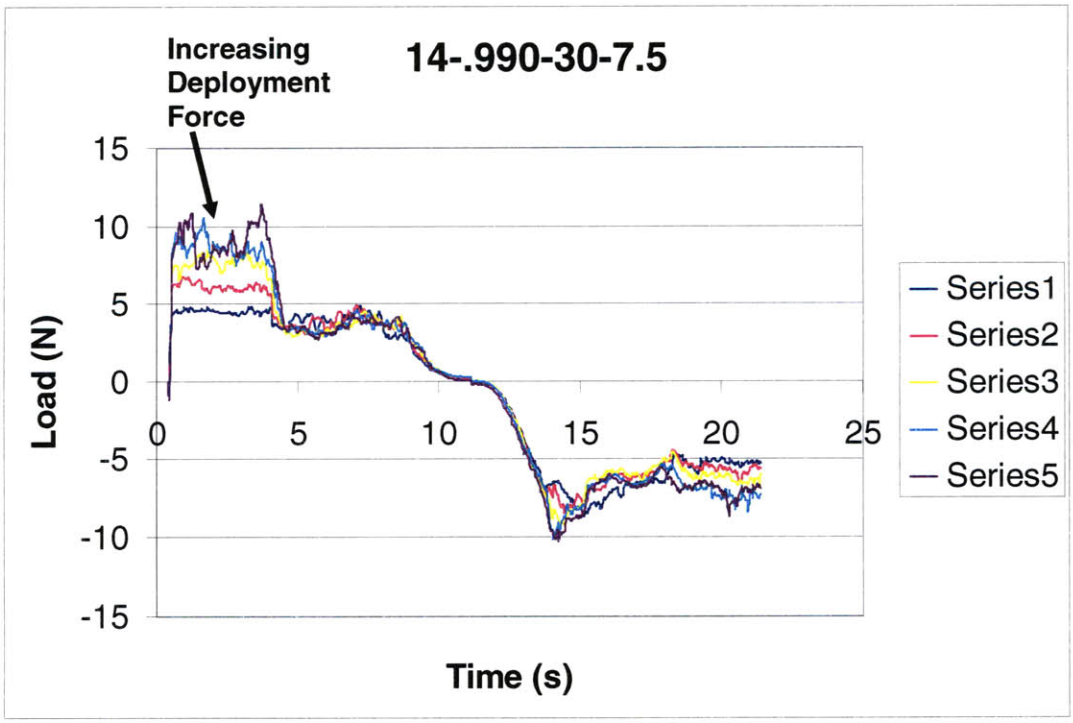

Figure 6.2: Increasing deployment forces observed in select test runs.

Analytical and Experimental Values of Deployment and Retraction Forces

To examine trends in deployment and retraction force for varying cannula diameter, stylet diameter, and bend radius, Figures 6.3-6.18 were produced that plot the deployment force as a function of the various combinations of cannula diameter, stylet diameter and bend radius. Maximum and minimum values from each of the five runs were recorded from each deployment/retraction plot (example shown in Figure 6.1), averaged and plotted. The analytical model shown in Chapter 4 is plotted against the experimental findings. The error bars on the experimental data represent the standard deviation between five experimental runs at each data point. Exponential curve fits are included in the plots to display trends so as to easily compare the experimental data to the analytical model.

Figures 6.3 to 6.10 plot force vs. bend radius for the deployment and retraction of all stylets through one cannula size. In these graphs, trends between force and bend radius and force and stylet diameter can be found. Some values are omitted from these plots because the retraction and deployment forces fell out the measurement bounds of the experiment load cell, or when the stylet was unable to fit into the cannula.

Forces for 14G Cannula and as a Function of Bend Radius and Stylet Diameter

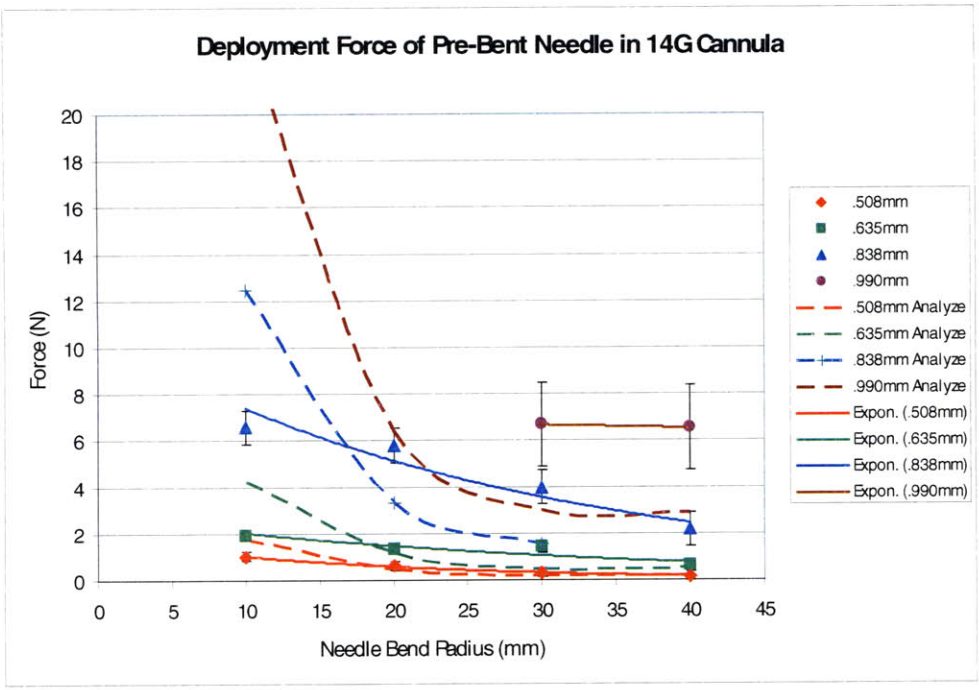

Figure 6.3: Deployment Force vs. Bend Radius plots for .508mm-.990mm stylets with 10mm-40mm bend radii deployed through a 14G cannula at 7.5mm/sec.

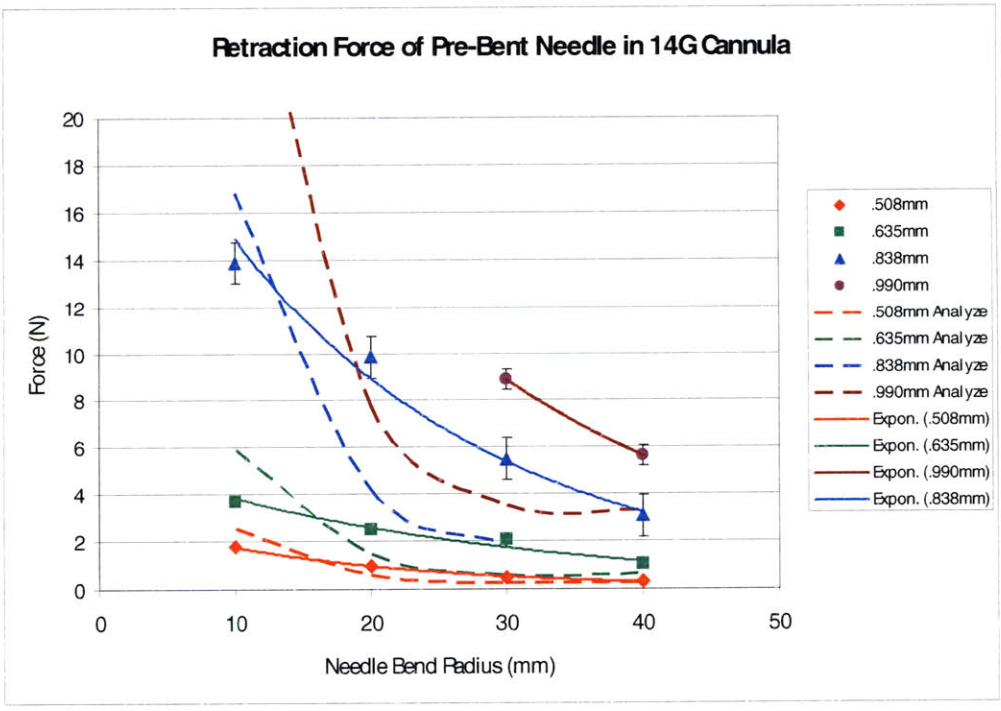

Figure 6.4: Retraction Force vs. Bend Radius plots for .508mm-.990mm stylets with 10mm-40mm bend radii deployed through a 14G cannula at 7.5mm/sec.

Forces for 16G Cannula and as a Function of Bend Radius and Stylet Diameter

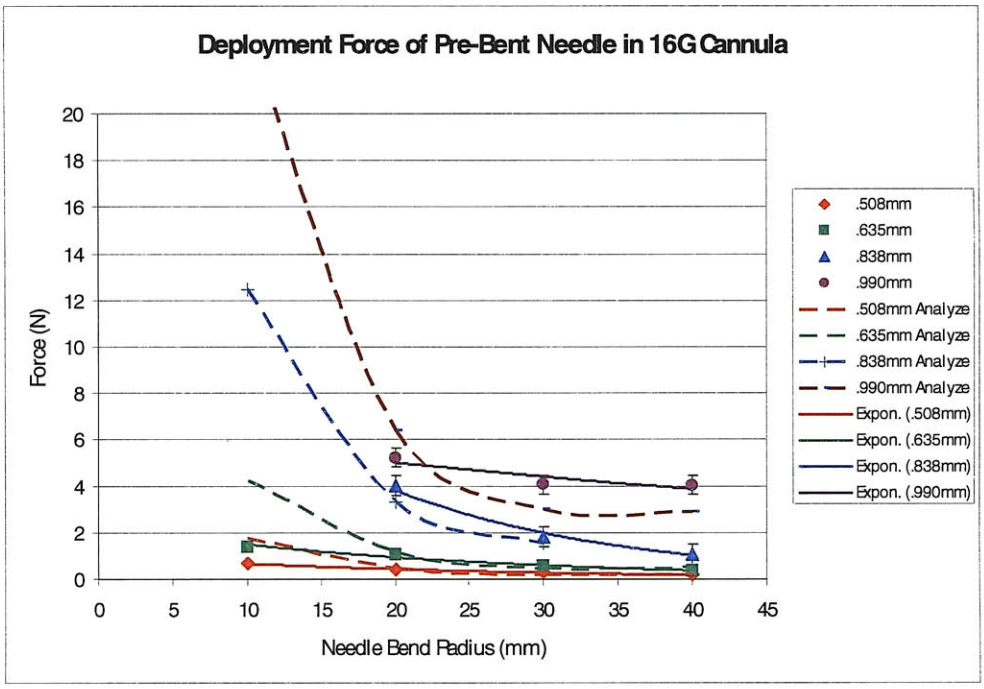

Figure 6.5: Deployment Force vs. Bend Radius plots for .508mm-.990mm stylets with 10mm-40mm bend radii deployed through a 16G cannula at 7.5mm/sec.

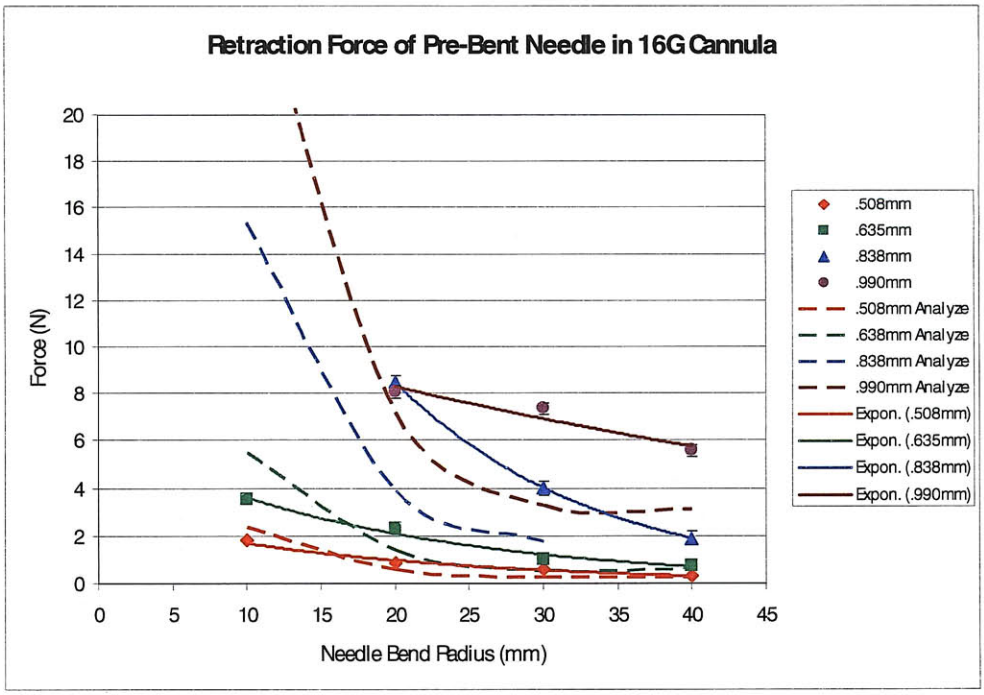

Figure 6.6: Retraction Force vs. Bend Radius plots for .508mm-.990mm stylets with 10mm-40mm bend radii deployed through a 16G cannula at 7.5mm/sec.

Forces for 18G Cannula and as a Function of Bend Radius and Stylet Diameter

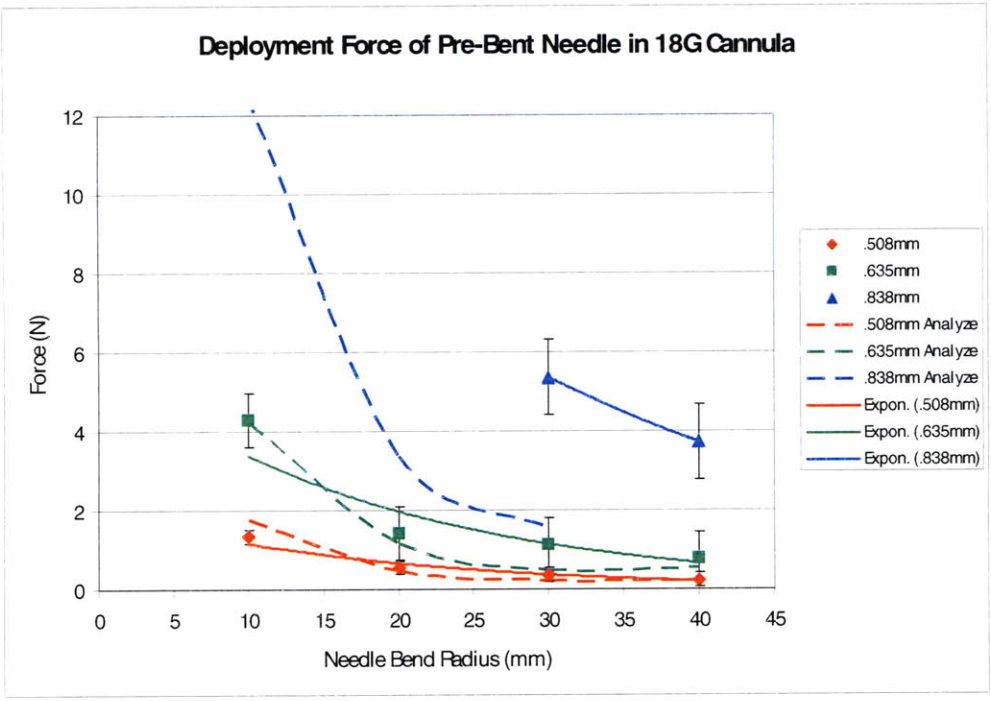

Figure 6.7: Deployment Force vs. Bend Radius plots for .508mm-.838mm stylets with 10mm-40mm bend radii deployed through an 18G cannula at 7.5mm/sec.

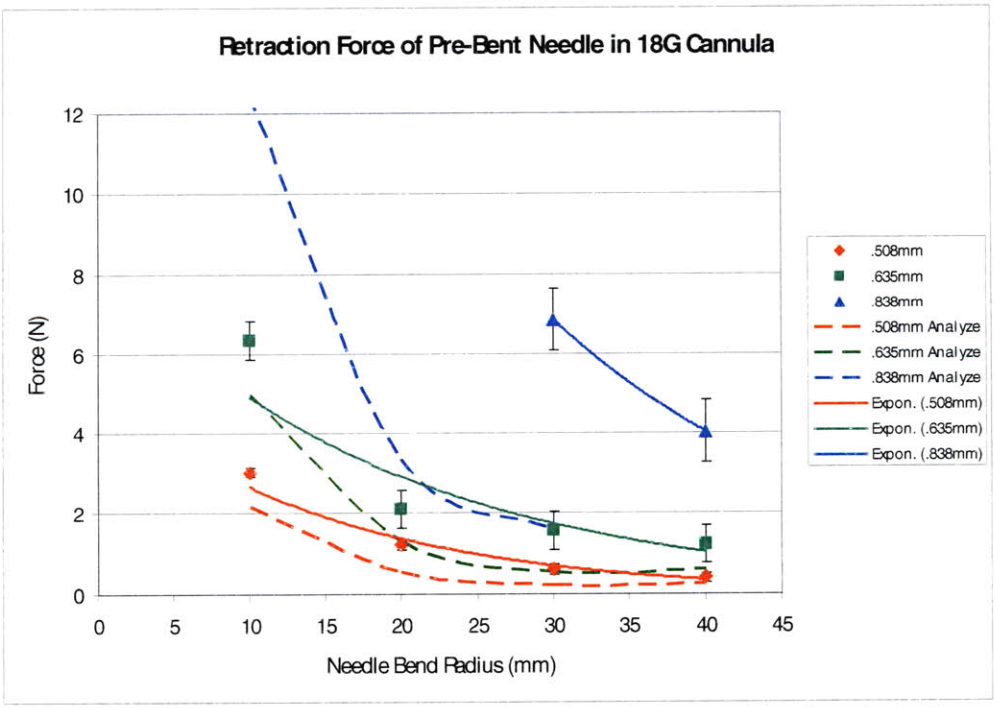

Figure 6.8: Retraction Force vs. Bend Radius plots for .508mm-.838mm stylets with 10mm-40mm bend radii deployed through an 18G cannula at 7.5mm/sec.

Forces for 20G Cannula and 0.508mm Stylet as a Function of Bend Radius

Note: only one line is plotted for the 20G Cannula because the .508mm stylets are the only ones small enough to pass through the inner diameter of this cannula.

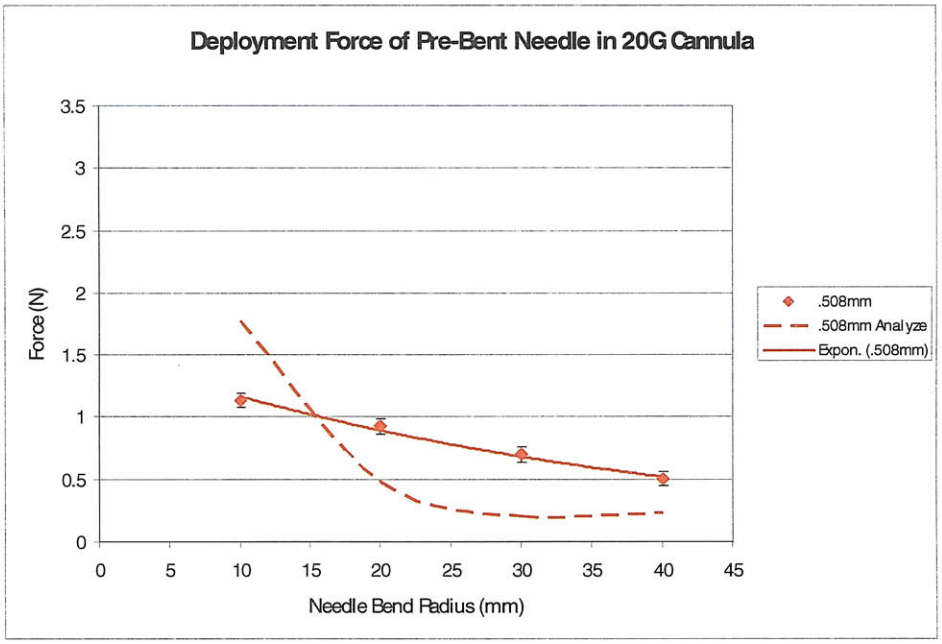

Figure 6.9: Deployment Force vs. Bend Radius plots for the .508mm stylet with 10mm-40mm bend radii deployed through a 20G cannula at 7.5mm/sec.

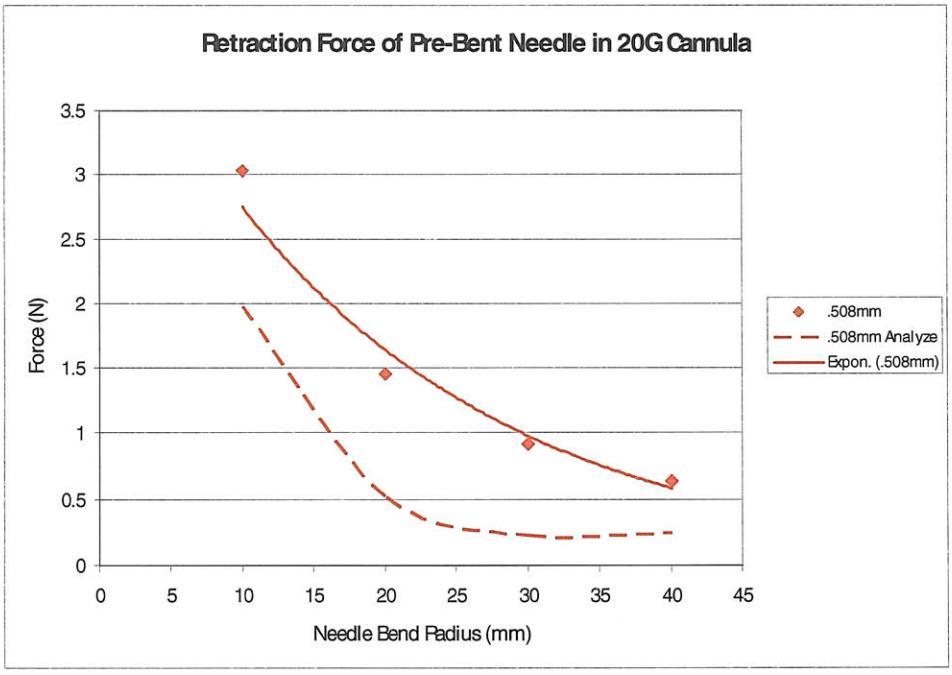

Figure 6.10: Retraction Force vs. Bend Radius plots for the .508mm stylet with 10mm-40mm bend radii deployed through a 20G cannula at 7.5mm/sec.

Examining Figures 6.3-6.10, it is shown that the retraction force of a stylet is always greater than the deployment force. For a given cannula diameter, force increases as stylet diameter increases and bend radius decreases. Additionally, slopes of the force vs. bend radius trend lines also increase as bend radius decreases. Included plots of the analytical model also appear to better fit the retraction and deployment measurements for smaller stylet diameters – specifically .508mm and .635mm.

Figures 6.11 to 6.18 plot force vs. bend radius for the deployment and retraction of all stylets of the same diameter. In these graphs, trends between force and bend radius and force and *cannula* diameter can be found. Some values are omitted from these plots because the retraction and deployment forces fell out the measurement bounds of the experiment load cell, or the stylet was unable to fit into the cannula. Only one analytical curve is displayed for deployment force plots in Figures 6.11, 6.13, 6.15, 6.17. As discussed in Chapter 4, maximum deployment force F is estimated as the friction force exerted against the stylet when it is fully retracted. Because the assumption was made that all stylets are straightened completely in all cases, cannula diameter does not affect the analytical model, and the deployment force is expressed as a single function of bend radius.

Forces for 0.508mm Diameter Wire as a Function of Bend Radius and Cannula

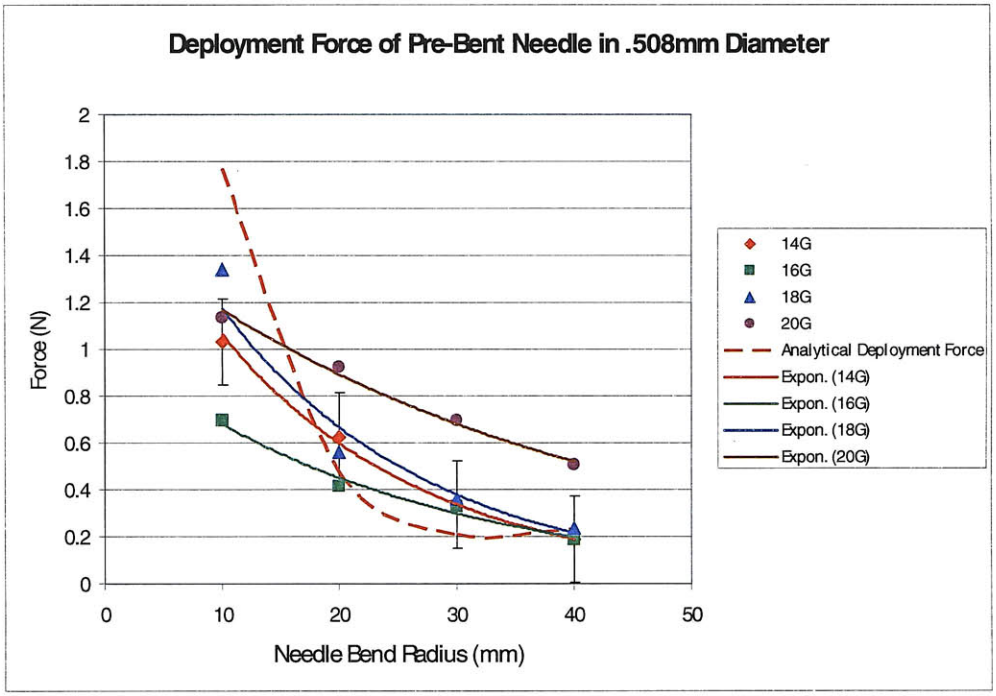

Figure 6.11: Deployment Force vs. Bend Radius plots for the .508mm stylet with 10mm-40mm bend radii deployed through a 14G, 16G, 18G, and 20G cannula at 7.5mm/sec.

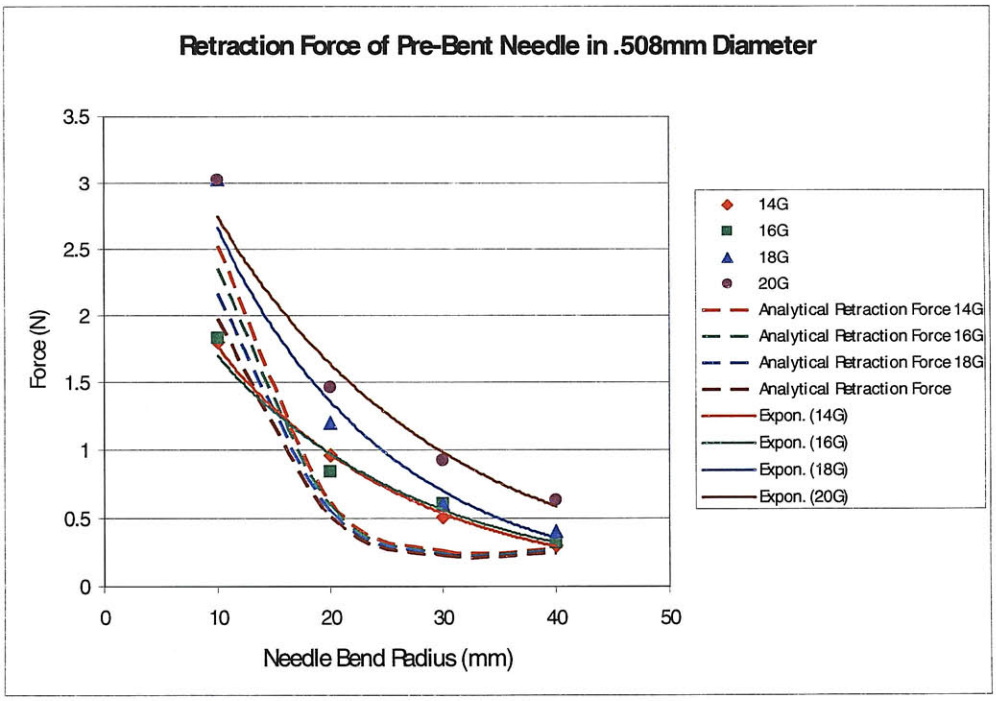

Figure 6.12: Retraction Force vs. Bend Radius plots for the .508mm stylet with 10mm-40mm bend radii deployed through a 14G, 16G, 18G, and 20G cannula at 7.5mm/sec.

Forces for 0.635mm Diameter Wire as a Function of Bend Radius and Cannula

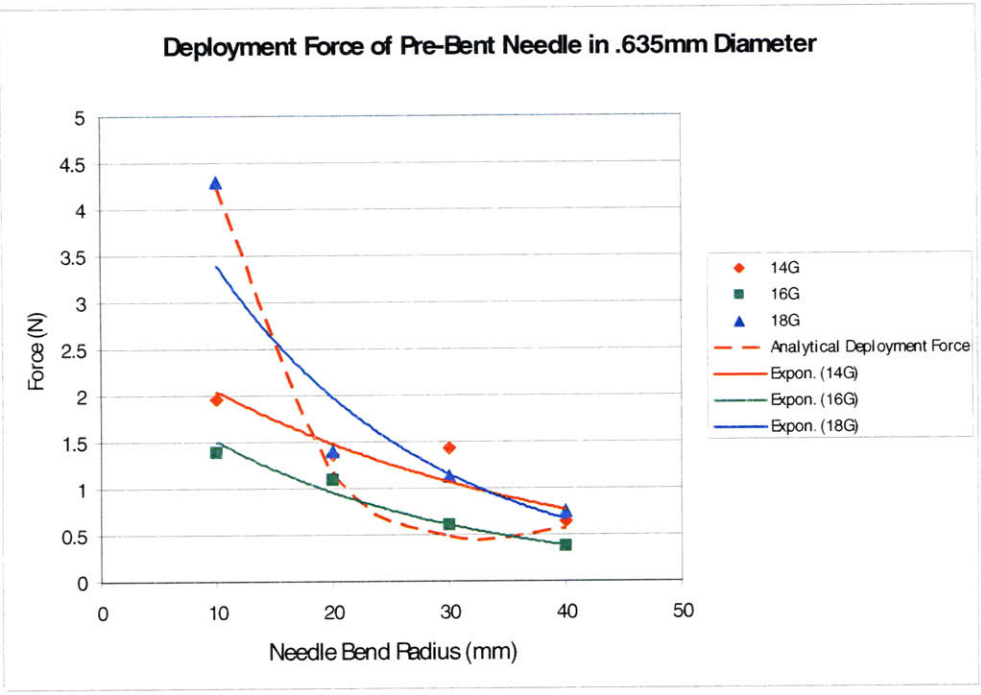

Figure 6.13: Deployment Force vs. Bend Radius plots for the .635mm stylet with 10mm-40mm bend radii deployed through a 14G, 16G, 18G, and 20G cannula at 7.5mm/sec.

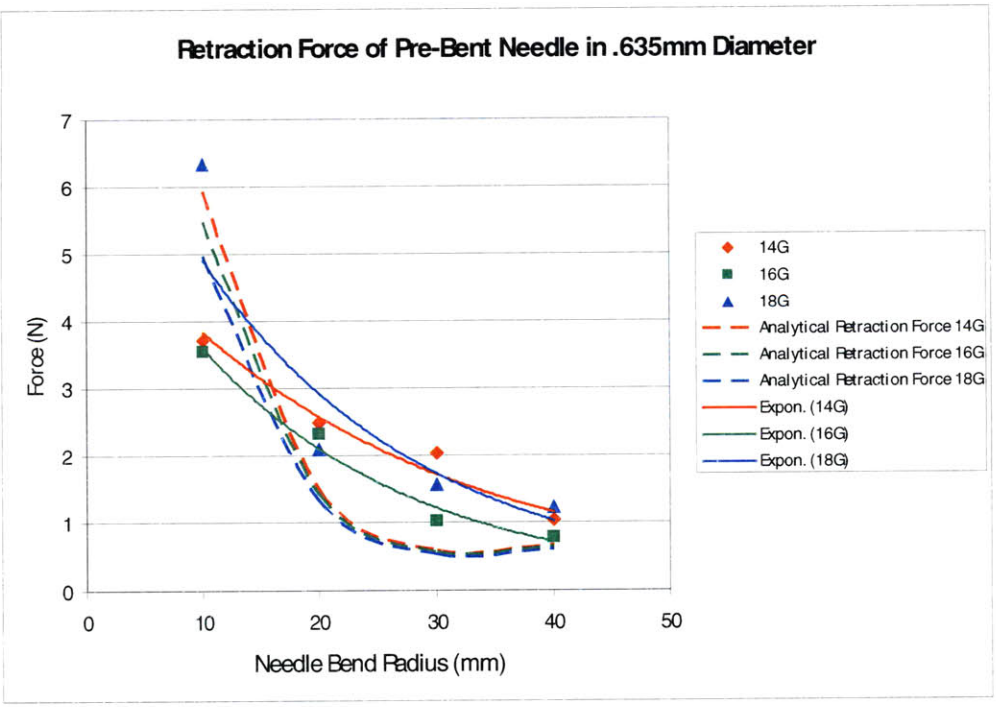

Figure 6.14: Retraction Force vs. Bend Radius plots for the .635mm stylet with 10mm-40mm bend radii deployed through a 14G, 16G, 18G, and 20G cannula at 7.5mm/sec.

Forces for 0.838mm Diameter Wire as a Function of Bend Radius and Cannula

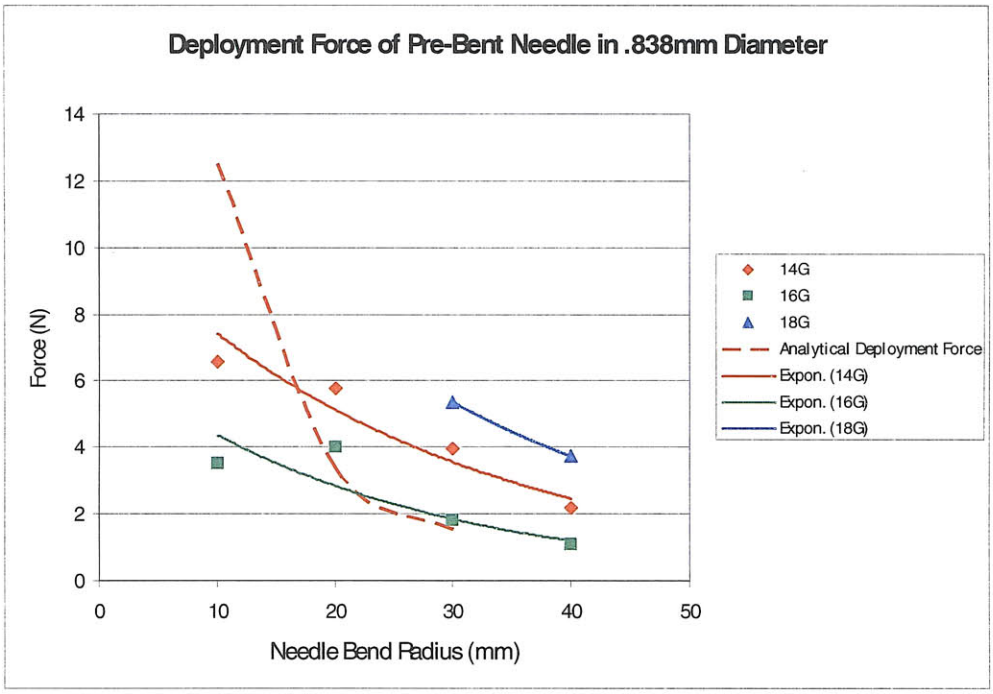

Figure 6.15: Deployment Force vs. Bend Radius plots for the .838mm stylet with 10mm-40mm bend radii deployed through a 14G, 16G and 18G cannula at 7.5mm/sec.

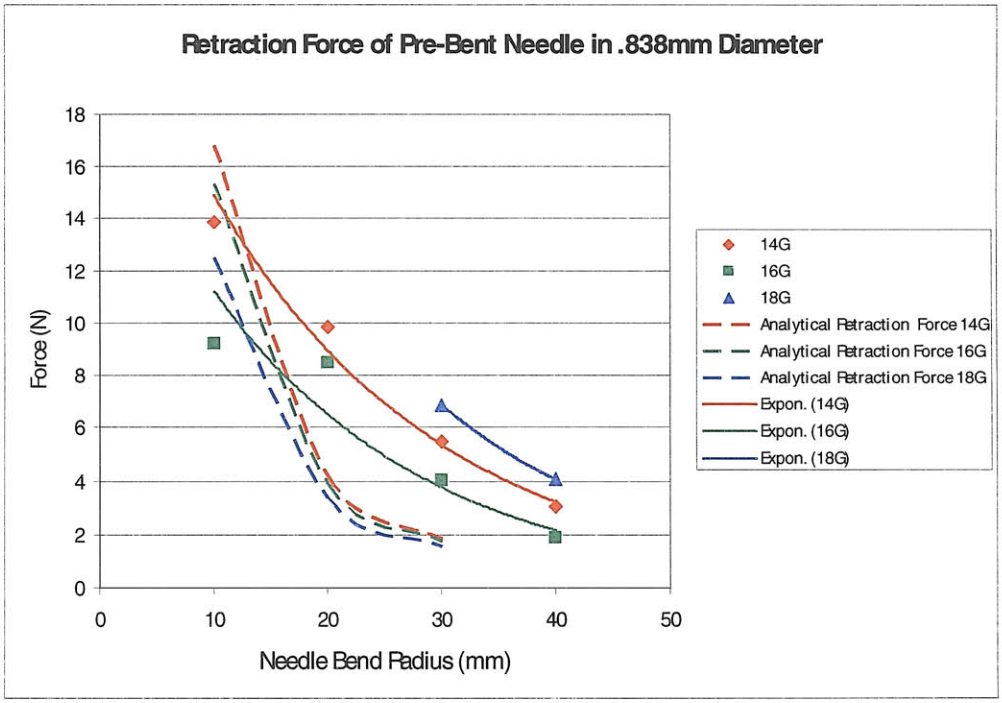

Figure 6.16: Retraction Force vs. Bend Radius plots for the .838mm stylet with 10mm-40mm bend radii deployed through a 14G, 16G and 18G cannula at 7.5mm/sec.

Forces for 0.990mm Diameter Wire as a Function of Bend Radius and Cannula

Note: only one line is plotted for the .990mm stylet because the 14G and 16G cannulas are the only ones large enough to pass the .990mm stylet through it.

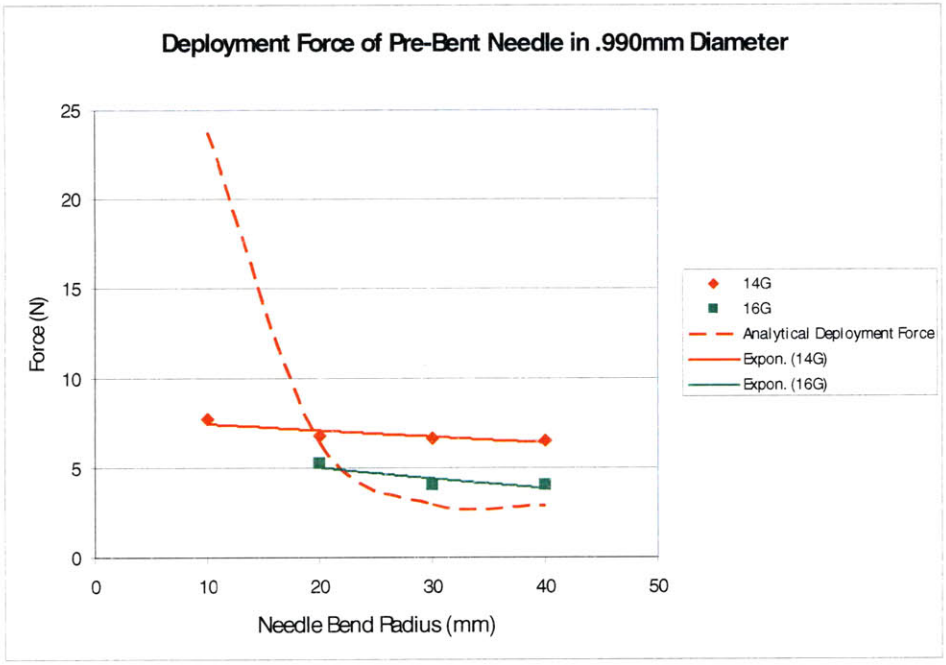

Figure 6.17: Deployment Force vs. Bend Radius plots for the .990mm stylet with 10mm-40mm bend radii deployed through a 14G and 16G cannula at 7.5mm/sec.

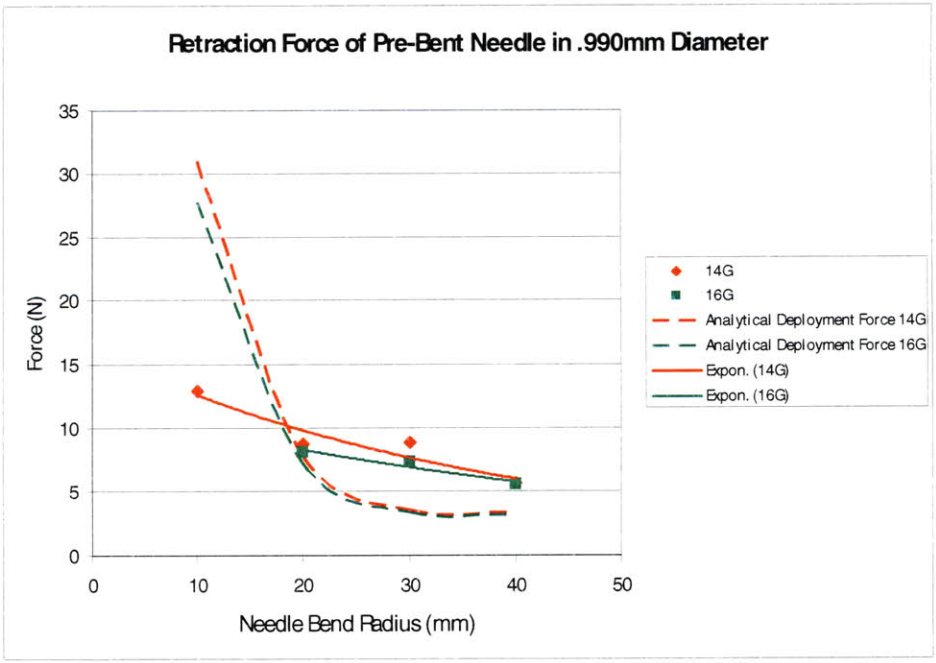

Figure 6.18: Retraction Force vs. Bend Radius plots for the .990mm stylet with 10mm-40mm bend radii deployed through a 14G and 16G cannula at 7.5mm/sec.

In Figures 6.11 to 6.18, a trend of increasing force with decreasing bend radius was observed for the majority of stylet and cannula diameters. Figures 6.11 to 6.18 also show that experimentally, the retraction and deployment do not necessarily increase or decrease with cannula diameter. Stylets drawn through the 16 gauge cannula consistently had the lowest deployment and retraction forces recorded. For example, the retraction force of the .838mm stylet with a 10mm bend radius drops from 18.8N to 8.49N between the 14G and 16G cannula tests. The analytical model also predicts that retraction forces will be reduced – albeit slightly – as cannula diameter decreases.

Comparing the analytical model of retraction force against experimental data, it was observed that the model fits experimental results best for small diameter stylets. With .508mm stylets (Figure 6.12), for example, the analytical model underestimates the load for the 20mm and 30mm data points, but effectively mirrors the increasing slope observed experimentally.

Chapter 7: Discussion

The analysis and experimental methodology described in Chapters 4 and 5 are intended to give designers analytical and experimental tools to design and prototype pre-curved steerable needles. The dimensions of cannulas and stylets that were prototyped in these experiments were based upon functional requirements and design parameters established in Chapter 3 for a steerable needle system designed to operate within the lung.

Experimental Methods

While most of the runs reliably and accurately recorded deployment and retraction loading, certain factors during the procedure were observed that contributed to variability in the measurements. The Needle Test Rig had to be aligned with the load cell by hand to allow the stylet to slide through the cannula which may have lead to the stylet and cannula not being perfectly concentrically aligned. For retraction and deployment loads above 10N, slipping between the stylet and the pin vice in the load cell was observed. When observed during experiments, the operator tightened the pin vice with pliers and marked the stylet to prevent slipping but some small slippage may have gone unobserved. Additionally, the pin vice used in the cannula within the test rig was adopted from a previous experiment [15]. The pin vice did not sit normal to the top plate of the fixture, and as a result, the cannula was sometimes observed pointing a few degrees off vertical. This angle could have potentially increased friction forces during experiments, and been the cause of the transitional force spikes observed in Figure 6.1. A stronger, more precise mechanism for gripping cannulas and stylets combined with a modified test fixture that automatically locates it relative to the load cell could improve experiment reliability.

The Nitinol wire manufacturing process was another challenging portion of the experiment that developed positively over the course of this thesis, but still has potential to be improved into a more robust system. Figures 6.3 to 6.10 show smooth trends between stylets of same diameter with different bend radii. This suggests that stylets heat treated together have consistent material properties, regardless of their position in the quench fixture. No tests were done to examine and compare the material properties between batches of stylets and heat treated vs. annealed material because insufficient

lengths of annealed and heat treated Nitinol was available to conduct tensile tests. Additionally, no method was established beyond visual examination and measuring the radius of stylet curvature with calipers for characterizing the bend geometries of heat treated stylets. Procedures for examining material properties before and after heat treatment and bend geometries before and after stylet deployment would be a valuable addition to Table 3.4 and Figure 4.1 which were used in the initial material selection and analysis process.

For small cannulas with large stylets inside (i.e. for the smallest ratio of area moment of inertia between the cannula and stylet) significant cannula tip deflection was observed as shown in Figure 7.1. This deflection will undoubtedly affect needle accuracy, along with the contact friction between the cannula and stylet developed in the analytical model. Developing a procedure for characterizing this curvature, and determining what is an acceptable level of deformation for a surgical system is extremely important for future development of a functional prototype.

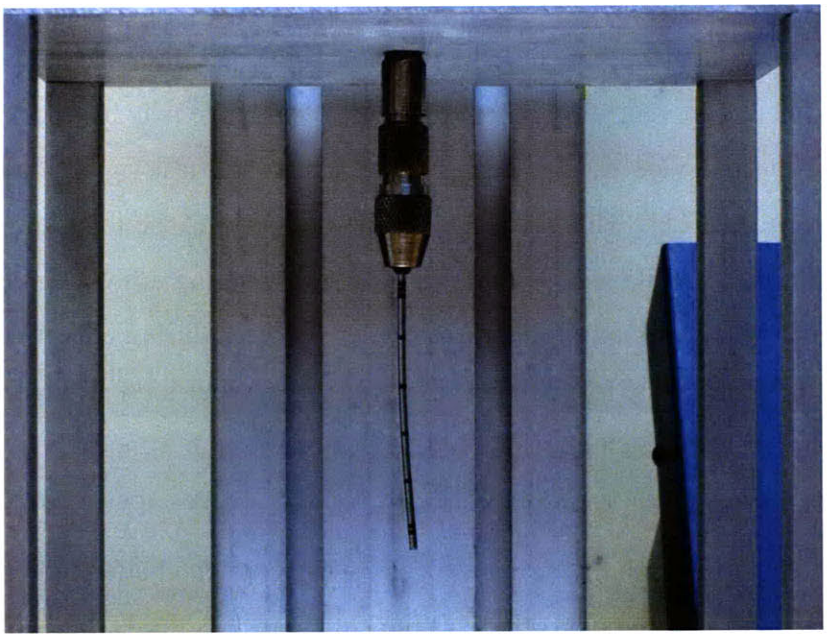

Figure 7.1: Tip deflection of cannula with pre-curved stylet retracted inside.

Analytical and Experimental Results

Given the assumptions made in developing the analytical model in Chapter 4, the analytical model fits the experimental data reasonably well. Examining Figures 6.11 to 6.18, a trend is observed where, for large bend radii, the predicted values are lower than expected, and at smaller bend radii, the slope of the curve dramatically increases and the analytical plot meets or crosses the experimental data. The best analytical/experimental fit shown is Figure 6.12, the retraction plot for .508mm diameter stylets. In Figure 6.12, the slopes of the analytical and experimental plots converge for bend radii near 10mm. Additionally, the analytical and experimental retraction force calculated for a bend radius of 40mm is nearly identical. One hypothesis for these close values is that the .508mm stylet with a 40mm bend radius is treated as being entirely elastic (as the calculated strain was less than the 0.7% transition strain (see Figure 3.1). As a result, no EI_{eff} was found for elastic/superelastic bending, and when linear elastic energy methods were applied, no component of the cross section was neglected as it is in the current analytical model (see Chapter 4). This was expected as we recognize that the assumptions made in calculating the location of the neutral axis require at least a .7% strain for the elastic/superelastic model to apply.

Three hypotheses were posed for why the analytical model fits more closely to small diameter stylets. (1) The small diameter stylets have the smallest area moments of inertia relative to the cannulas (see Table 4.1), and therefore, these stylets will deform the cannula least and will deform in a way closest to the modeling assumption of an infinitely stiff cannula that completely straightens the stylet. (2) The strain in the small diameter stylets is the lowest and so any errors from calculating an EI_{eff} based on the final deformed position will lower as the majority of stress in the cross section will be elastic. (3) The small diameter stylets have a greater ratio of bend radius to wire diameter than other samples fit best with the large bend radius assumptions made in the analytical model in Chapter 4.

Overall, the analytical model developed in Chapter 4 gave us a good understanding of the principles and phenomena at play as a curved beam is drawn into a straight cannula. Geometric models to evaluate friction and retraction forces were created, and

also for stylets with small bend radii. Several gross assumptions were made in the evaluation of the model, including a constant value for effective stiffness, strain calculations based on large radii of curvature, a constant stress distribution within the stylet, and an inelastic cannula. All of these factors change as the stylet is deformed inside the cannula, and future analytical models could incorporate deformation-based equations to more accurately apply energy methods.

Chapter 8: Conclusion

It has been shown experimentally that pre-curved Nitinol stylets can be deployed as steerable needles at force levels that are reasonable for a telerobotic system that is under development that is capable of needle distal tip manipulation in the body. Interviews with surgeons and prior literature reviews indicated that the pre-curved stylet strategy was a robust design, with few components that could be easily prototyped. Analytical models were developed to (1) understand what material properties are required to recover from the imposed strains, (2) compare stylet stiffness relative to each other and the cannulas, and (3) calculate the deployment and retraction forces required for moving the stylet relative to the cannula The data collected for 48 permutations of stylet diameter, stylet bend radius, and cannula gauge were compared to the analytical model.

Retraction forces were measured between .277 and 13.9N, and deployment forces were measured between .191 and 6.95N. For a given cannula it was found that force increases as stylet diameter increases and bend radius decreases. The analytical model better matched the experimental retraction and deployment measurements for the smaller stylet diameters (0.508 and 0.635 mm) with low friction, retraction and deployment forces. This was expected as the assumptions made for the elastic-perfectly plastic model have the least effect as these diameters had the minimum strain and thus any errors in calculating the effective *EI* of the beam were also minimized. It was found that the retraction and deployment force do not necessarily increase or decrease with cannula diameter and it was found that the stylets drawn through the 16 gauge cannula consistently had the lowest deployment and retraction forces recorded across the four cannulas tested.

Future Work

Future work on pre-bent steerable stylets includes improving both experimental and analytical methods to better characterize the behavior of this steerable needle strategy. For future experiments, improved accuracy could be achieved by (1) validating Nitinol heat treatment process to assure consistent material properties between stylet batches, (2) improving alignment methods between the ADMET Universal Testing Machine and the Needle Test Rig to better assure stylet/cannula concentricity and (3)

measuring cannula deflection when a curved stylet is inserted inside it. For future analytical models, improvements would be (1) a model that took into account the variation in the position of the neural axis and curvature as a function of force or deflection, (2) including the effect of an elastic (not perfectly rigid) cannula and (3) a finite element model of a curved beam being withdrawn into a cannula to validate the assumptions of the analytical model.

Experiments and analytical models validating this strategy's effectiveness and accuracy when deployed in gel and tissue are also critical for identifying whether this strategy is adequate for designing a device capable of accurate distal tip needle manipulation.

References

[1] Walsh, C., Hanumara, N., Slocum, A., Shepard, J., Gupta, R. A Patient-Mounted, Telerobotic Tool for CT-Guided Percutaneous Interventions, ASME Journal of Medical Devices, 2(1): 2008.

[2] Advantages of the Cool-Tip™ RF Ablation System. Valleylab, Tyco Healthcare Group LP, 2007. http://www.cool-tiprf.com/pdf/cool-tip_brochure.pdf

[3] Needles for Biopsy and Special Purpose, Cook Medical, 2008. http://cookmedical.com/di/content/mmedia/PI-BM-BSPNMP-EN-200811.pdf

[4] Cool-Tip™ RF Tissue Ablation System. Valleylab, Tyco Healthcare Group LP, 2004. http://www.cool-tiprf.com/pdf/cool-tip_ss.pdf

[5] Pakter Curved Needle Set. Cook Medical, 2001. http://www.cookmedical.com/di/content/mmedia/CURVE201.pdf

[6] Osteo-Site® Bone Access Products. Cook Medical, 2005. http://www.cookmedical.com/di/content/mmedia/OSBB305.pdf

[7] Introducing the Seeker Biopsy Needle. PneumRx. http://www.pneumrx.com/Components/fna_v3.pdf

[8] Cosman RF Cannulae. Cosman Medical, 2006. http://www.cosmanmedical.com/Media/cc.pdf

[9] Nitinol, Fort Wayne Metals. http://fwmetals.com/specsheet_pdfs/nitinol.pdf

[10] Stainless Steel. AZo Materials, 2009. http://www.azom.com/Details.asp?ArticleID=965

[11] Beer et. al. *Mechanics of Materials*. McGraw Hill, New York, NY, 1981.

[12] D.B. Wallace. Basic Stress Equations. http://www.eng.uah.edu/~wallace/mae466/DOC/bas_str.pdf

[13] R.J. Webster, J.M. Romano, N.J. Cowan. Mechanics of Precurved-Tube Continuum Robots. *IEEE Transactions on Robotics*. 25, No. 1, 6-78, 2009.

[14] D. Stoeckel and W. Yu. Superelastic Ni-Ti Wire. Nitinol Development Corporation, 1991. http://www.nitinol.info/pdf_files/056.pdf

[15] Bassett, E.K. Buckling and Friction-Based Linear Motion Clutch with Application to Medical Devices. Masters Thesis. Massachusetts Institure of Technology, 2008.

[16] Hammerslag, Gary R. (Dana Point, CA), Hammerslag, Julius G. (San Juan Capistrano, CA), 1994. Steerable medical device. United States. Pilot Cardiovascular Systems, Inc. (San Clemente, CA). 5308324 http://www.freepatentsonline.com/5308324.html

[17] Mogul, Jamil (2665 Somerset Park Cir., San Jose, CA, US), 2007. Steerable diagnostic catheters. United States. 7269453 http://www.freepatentsonline.com/7269453.html

[18] Gibson, Charles A. (Malden, MA), 2001. Steerable catheter. United States. C.R. Bard, Inc. (Murray Hill, NJ). 6224587 http://www.freepatentsonline.com/6224587.html

[19] Kuhle, William G. (815 14th St. Apt. A, Santa Monica, CA, 90403-1759), 1999. Biopsy needle with flared tip. United States. 5938635 http://www.freepatentsonline.com/5938635.html

[20] S. Okazawa; R. Ebrahimi; J. Chuang; S.E. Salcudean; R. Rohling, "Hand-held steerable needle device," *Mechatronics, IEEE/ASME Transactions on* , vol.10, no.3, pp.285-296, June 2005 URL: http://ieeexplore.ieee.org/stamp/stamp.jsp?arnumber=1461405&isnumber=31442

[21] Sauer, Jude (Rochester, NY), 2007. Ergonomic Needle Tissue Harvesting Instrument Not Requiring a Stylet. United States. 2007/0167868 http://www.google.com/patents?id=YLWAAAAAEBAJ

[22] Heaven, Malcolm D. (Hopewell, NJ), Klapper, Robert C. (Sherman Oaks, CA), 1994. Steerable surgical devices. United States. Advanced Surgical Inc. (Princeton, NJ). 531852 http://www.freepatentsonline.com/5318528.html

[23] Cunningham, Miles G. (28 Harvard St., Unit 2, Charlestown, MA, 02129), 1998. Systems and methods for delivering therapeutic agents to selected sites in a subject. United States. 5792110 http://www.freepatentsonline.com/5792110.html

[24] Pakter, Robert L. (Mill Valley, CA), Morris, Edward J. (Bloomington, IN), 2003. Hollow, curved, superlastic medical needle. United States. Cook Incorporated (Bloomington, IN). 6592559 http://www.freepatentsonline.com/6592559.html

[25] Daum, Wolfgang Rudolf (Neu Schlagdorf, DE), 2003. Deflectable needle assembly. United States, Daum GmbH (DE). 6572593 http://www.freepatentsonline.com/6572593.html

Appendix 1: Prior Literature Search Findings

Cannula Mechanisms

Mechanism 1: "Steerable Medical Device" Pat No. 5308324

Mechanism features a tubular flexible housing made from a tightly coiled spring. The housing orientation can be manipulated by deflecting a "steering post" (23) enclosed within it. The steering post is deflected with three deflection wires (28). The deflection wires are loaded in tension and/or compression by changing the orientation of the deflection plate (34).

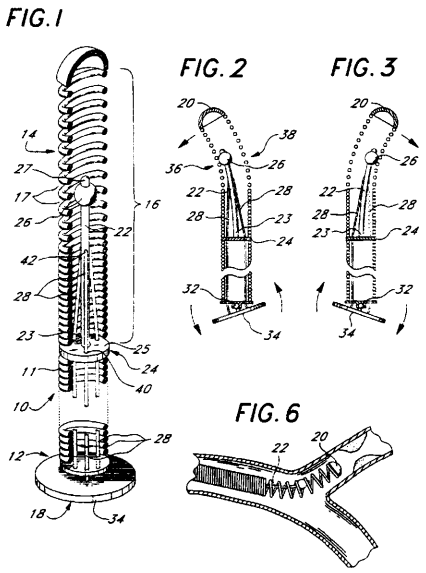

Figure A1.1: "Steerable Medical Device" Pat No. 5308324

Mechanism 2: "Steerable Diagnostic Catheters" Pat No. 7269453

Mechanism features a deployable structure – a "basket catheter" – that deploys from the end of a flexible member by sliding the connecting joint (370) toward the distal end of the apparatus.

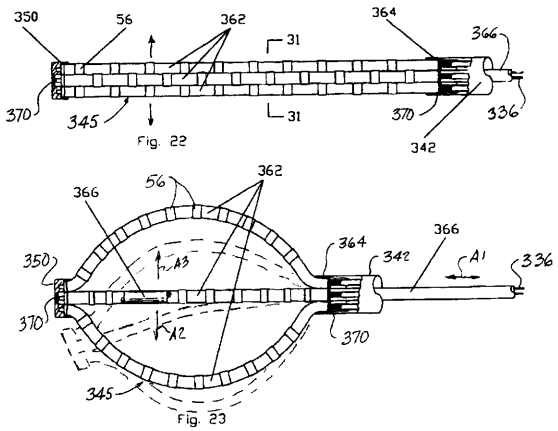

Figure A1.2: "Steerable Diagnostic Catheters" Pat No. 7269453

Mechanism 3: "Steerable Mechanism for Bi-Directional Catheter" Patent App. No. 2008/025540

Mechanism features a bending tube that is displaced with two puller wires (32a, b) that are spring loaded and routed through a pulley system. To achieve bending in desired segments, the catheter body is divided into multiple components, a stiff polymer braid-reinforced main body (12) and short flexible segments of tubing (14) located at the distal end of the device.

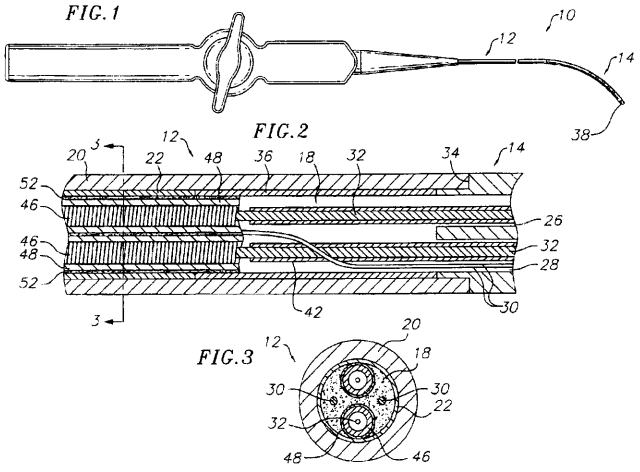

Figure A1.3: Steering Mechanism for Bi-Directional Catheter

Mechanism 4: "Steerable Catheter" Pat. No. 6224587

Mechanism incorporates a long tubular body containing segments that change angle and radius of curvature by applying tension to coaxial pull wires (29). Using this technique, straight sections of shaft can be bent into c-curves (25).

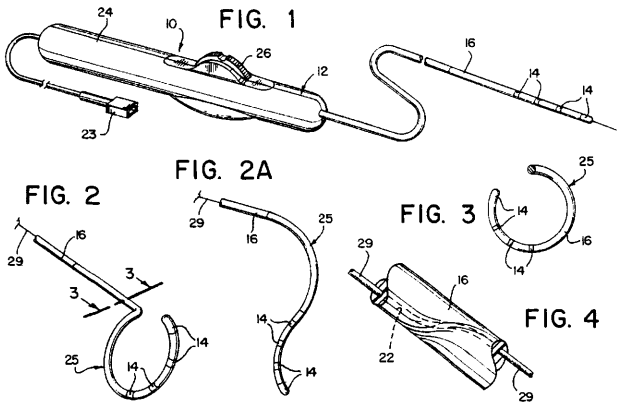

Figure A1.4: "Steerable Catheter" Pat. No. 6224587

Biopsy and Tissue Sampling Technologies

Mechanism 5: "Biopsy Needle with Flared Tip" Pat. No. 5938635

Mechanism described has flared tips on the end of standard biopsy needles. The flared tip causes the needle to travel in an arc as it cuts through tissue, allowing it to bend within a patient.

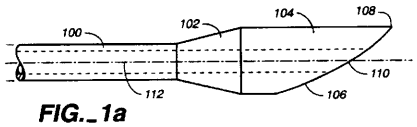

FIG._1a

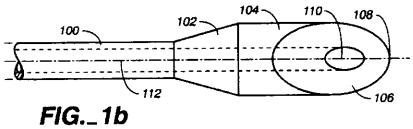

FIG._1b

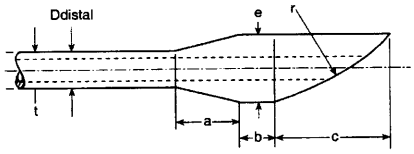

FIG._1c

Design Parameter	Example Measurement (IN.)
a	0.0125
b	0.050
c	0.050
Ddistal	0.025
e	0.050
t	0.006
r	0.50

Table 1

Figure A1.5: "Biopsy Needle with Flared Tip" Pat. No. 5938635

Mechanism 6: "Hand-Held Steerable Needle Device," Ebrahimi US 2004/0133168

Mechanism described has two concentric cylinders, a stiff hallow outer cylinder and a narrow, flexible, curved inner cylinder. Steering is accomplished by deploying the bent inner stylet from the straight cannula, and then inserting the entire needle system deeper into tissue. The reaction forces acting on the curved tip of the needle system causes the cannula and stylet to curve. Rotating the inner cylinder controls which direction the system will bend. Mechanism provides three degrees of freedom in a cylindrical reference frame, z, r, and θ.

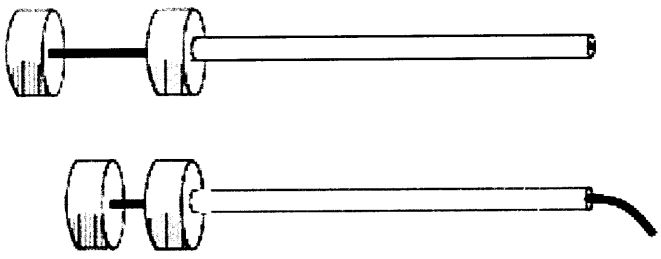

Figure A1.6: "Hand-Held Steerable Needle Device," Ebrahimi

Mechanism 7: "Ergonomic Needle Tissue Harvesting Instrument Not Requiring a Stylet" Pat. App. No. 2007/0167868

Mechanism described has a pivoting head mechanism that allows a needle to enter tissue at an appropriate angle while the operator holds the pistol grip handle in a comfortable position. Surgeon manipulates medical device with two hands, one controlling needle actuation, the other controlling vacuum suction and needle oscillation used in tissue harvesting procedure.

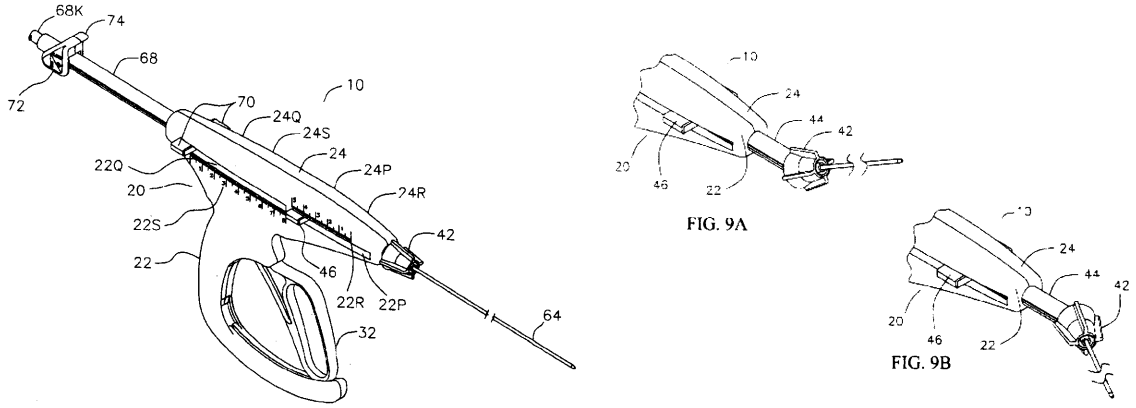

Figure A1.7: "Ergonomic Needle Tissue Harvesting Instrument Not Requiring a Stylet" Pat. App. No. 2007/0167868

Mechanism 8: "Steerable Surgical Devices," Pat. No. 5318528

Mechanism described has an assembly of pre-bent cylindrical tubes (2, 3). When bend radii of inner and outer tubes are pointing in the same direction, the device naturally bends. When the bend radii in each tube are oriented in opposite directions, however, both tubes are deformed and the device straightens into a line.

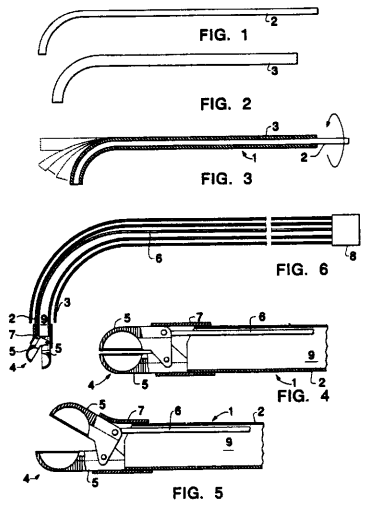

Figure A1.8: "Steerable Surgical Devices," Pat. No. 5318528

Concentric Component Steerable Needles

Mechanism 9: "Systems and Methods for Delivering Therapeutic Agents to Selected Sites in a Subject," Pat. No. 5792110

Mechanism described has a concentric cannula and stylet. The distal end of the cannula tube is bent and exits from the side wall of the cannula. The stylet, being much smaller in diameter than the cannula bends along this path and deploys at an angle θ.

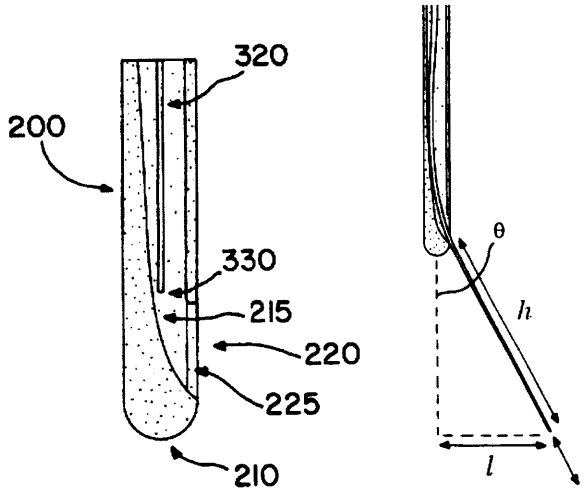

Figure A1.9: "Systems and Methods for Delivering Therapeutic Agents to Selected Sites in a Subject," Pat. No. 5792110

Mechanism 10: "Hollow, Curved, Superlastic Medical Needle," Pat No. 6592559B1

Mechanism described has a pre-bent inner, superelastic stylet within a rigid, straight cannula. Inner stylet is bent at a constant radius, r. With axial displacement of the cannula and stylet (z_{can} and z_{styl}) and rotation of the stylet (θ), three degrees of freedom is achieved. The distal tip of the stylet can contact any point within a control volume, like the vertebrae disc shown at right.

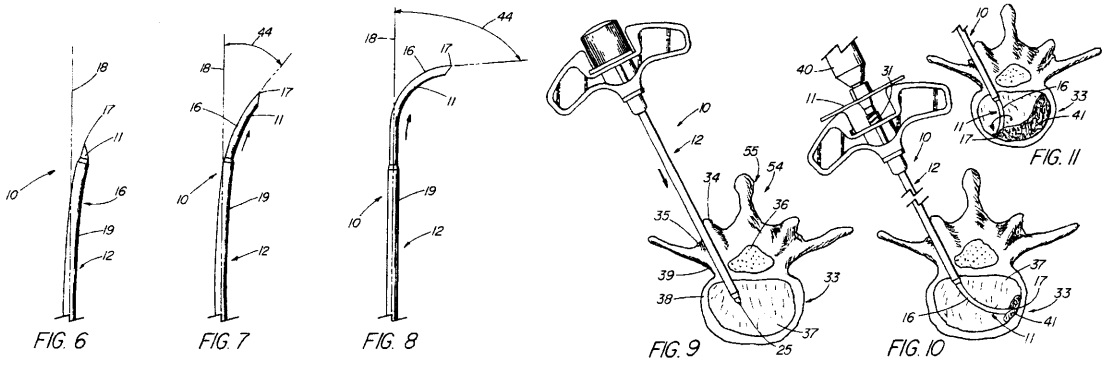

Figure A1.10: "Hollow, Curved, Superlastic Medical Needle," Pat No. 6592559B1

Mechanism 11: "Deflectable Needle Assembly," Pat No. US 6,572,593

Mechanism contains three concentric components: a straight outer cannula, a pre-bent inner catheter, and a stylet. Deploying the pre-bent catheter through the lumen of the cannula causes the cannula to bend in a desired orientation and steered toward a target.

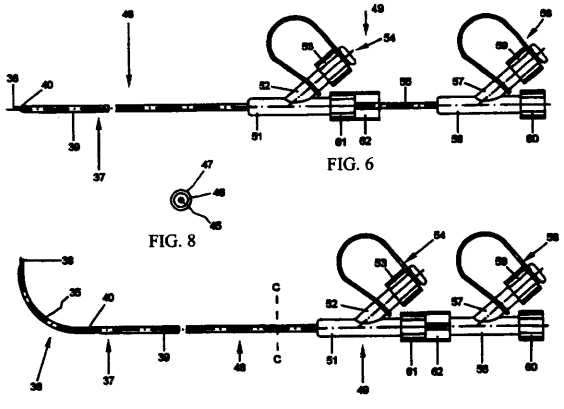

Figure A1.11: "Deflectable Needle Assembly," Pat No. US 6,572,593

Appendix 2: Manufacturing Curved Needles

Three versions of the Nitinol quench fixture were designed and prototyped to form pre-bent stylets. The first, shown in Figure A2.1, was three steel plates; two solid outer plates that held the inner outline plate in place. Six screws were needed to hold the original design together, one at each corner of the outline plate, and two on the wire locating plate (See Figure 5.1 for quench fixture layout diagram). When the heat treatment procedure tests were done with the original fixture, bowing was observed in the outer plates. It was hypothesized that non-uniformities within the steel caused some parts of the fixture to contract before others, resulting in bending and separation of the fixture.

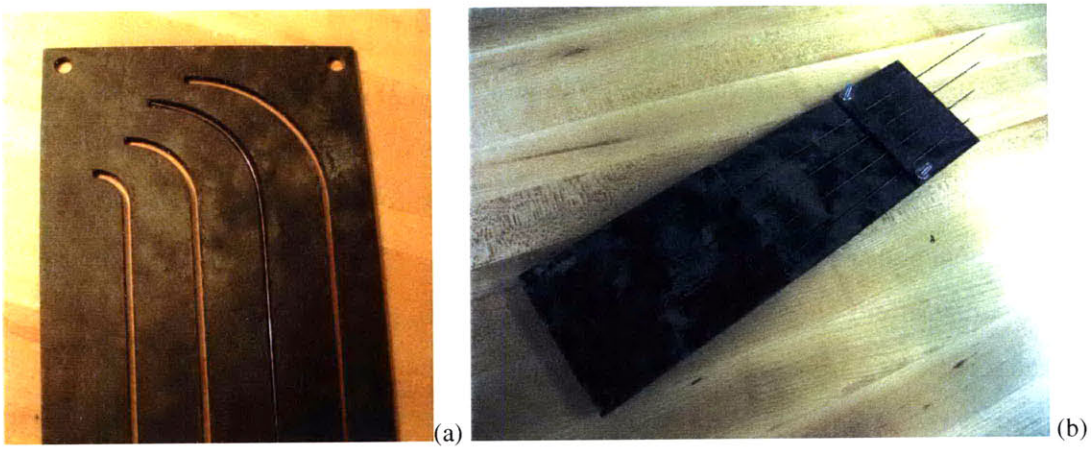
(a) (b)

Figure A2.1: Original outline plate (a) and quench fixture (b).

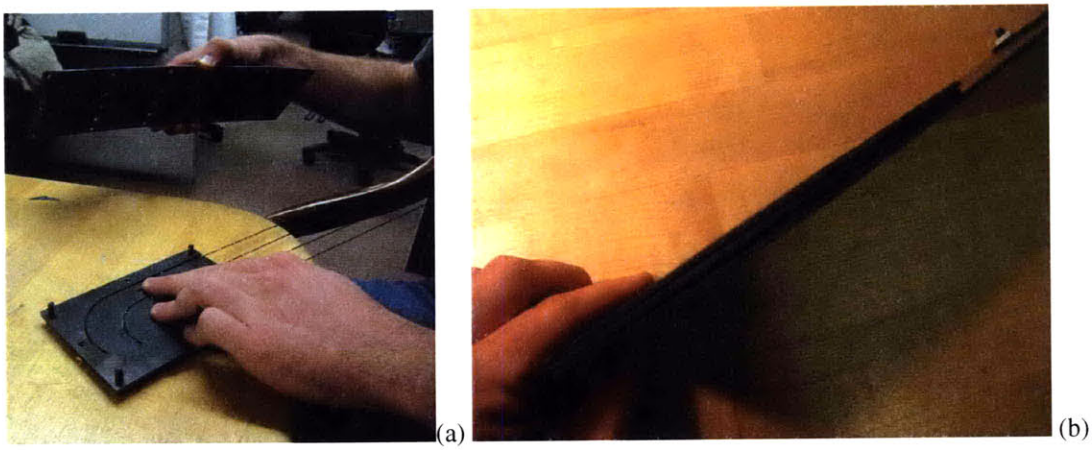
(a) (b)

Figure A2.2: Assembly of quench fixture (a), and bowing observed after quench. (b)

A more aggressive hole pattern was adopted to better locate the plates with respect to each other, but warping was still observed during quench tests. To eliminate warping,

thick steel "picture frames" that were dimensioned using St. Venant's principle, were added to the fixture.

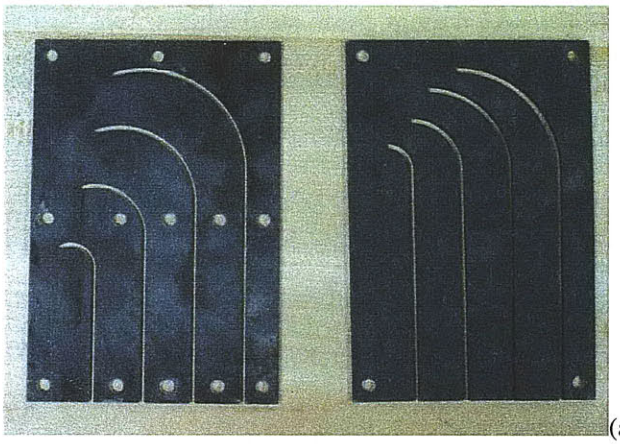
(a)

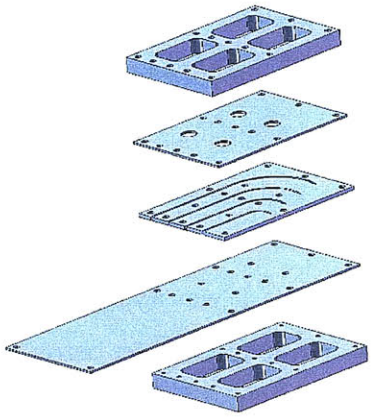
(b)

Figure A2.3: New outline plate with aggressive screw hole pattern to reduce warping (a). Original picture frame design. (b)

The picture frames succeeded in reducing fixture warping to an unnoticeable level. Wires quenched with the picture frames, however, did not maintain their imposed radius of curvature after being quenched and removed from the fixture. It was hypothesized that the added thermal mass and absence of warping meant that the quench could not cool the Nitinol wires rapidly enough, and the desired material properties were not achieved, resulting in spring back.


(a)

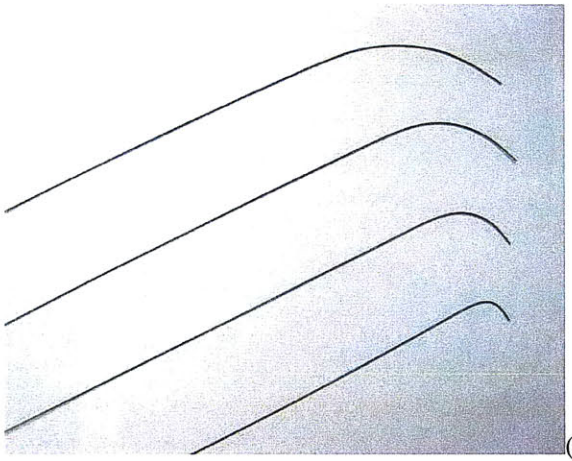
(b)

Figure A2.3: Original picture frame fixture layout (a), and poorly quenched stylets from original picture frame (b)

To address this problem, narrow slots were cut into the outer plates, or vent plates, of the fixture, allowing water to flow directly around the wires being held in place. This fixture successfully produced 16 curved stylets that exhibited no spring back on upon removal from the fixture, and maintained their shape after being drawn into cannulas.

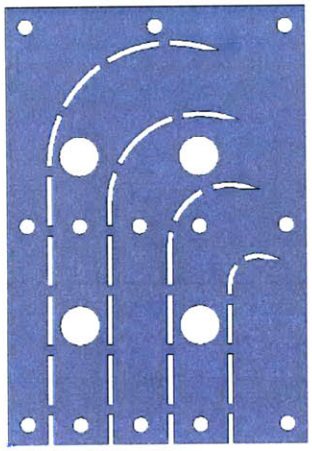

(a)

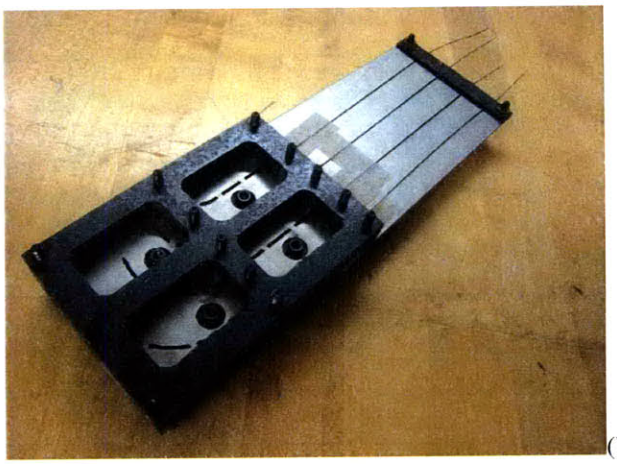

(b)

Figure A2.4: Vent plate designed to allow water to flow over wires in the fixture (a). Fully assembled fixture with picture frames and vent plates (b).

Appendix 3: Experimental & Analytical Results Tables

Experimental Results

The following values were recorded from each test run of the Deployment Retraction Force Test: (1) Maximum Deployment Force, (2) Standard Deviation between Deployment Force Runs, (3) Maximum Retraction Force, (4) Standard Deviation between Retraction Force Runs. These values are plotted and compared to analytically determined values in Chapter 6.

Table A3.1: Deployment-Retraction Test Results

Cannula Gauge	Stylet Diameter (mm)	Bend Radius (mm)	MAX D-Force (N)	S-DEV MAX D-Force (N)	MAX R-Force (N)	S-DEV MAX R-Force (N)
14	0.99	40	6.560	0.682	5.630	0.247
14	0.99	30	6.700	1.817	8.877	0.448
14	0.99	20	6.776	1.352	8.756	0.535
14	0.99	10	7.748	0.629	12.890	0.533
14	0.8382	40	2.198	0.246	3.062	0.083
14	0.8382	30	3.991	0.726	5.501	0.427
14	0.8382	20	5.806	1.046	9.844	0.882
14	0.8382	10	6.594	0.712	13.878	1.027
14	0.635	40	0.655	0.075	1.043	0.059
14	0.635	30	1.436	0.053	2.039	0.026
14	0.635	20	1.364	0.260	2.483	0.215
14	0.635	10	1.961	0.064	3.711	0.047
14	0.508	40	0.188	0.011	0.304	0.003
14	0.508	30	0.338	0.041	0.510	0.016
14	0.508	20	0.629	0.058	0.962	0.044
14	0.508	10	1.031	0.185	1.801	0.013
16	0.99	40	4.041	0.300	5.574	0.111
16	0.99	30	4.071	0.234	7.342	0.244
16	0.99	20	5.241	0.401	8.045	0.160
16	0.99	10				
16	0.8382	40	1.096	0.039	1.908	0.063
16	0.8382	30	1.815	0.093	4.006	0.286

Cannula Gauge	Stylet Diameter (mm)	Bend Radius (mm)	MAX D-Force (N)	S-DEV MAX D-Force (N)	MAX R-Force (N)	S-DEV MAX R-Force (N)
16	0.8382	20	4.011	0.434	8.491	0.272
16	0.8382	10	3.504	0.130	9.198	0.134
16	0.635	40	0.376	0.021	0.766	0.009
16	0.635	30	0.608	0.017	1.026	0.009
16	0.635	20	1.090	0.071	2.328	0.060
16	0.635	10	1.389	0.045	3.554	0.054
16	0.508	40	0.192	0.008	0.321	0.011
16	0.508	30	0.330	0.028	0.600	0.040
16	0.508	20	0.416	0.018	0.838	0.011
16	0.508	10	0.700	0.028	1.826	0.010
18	0.8382	40	3.731	0.324	4.052	0.225
18	0.8382	30	5.368	0.962	6.851	0.776
18	0.8382	20				
18	0.8382	10				
18	0.635	40	0.762	0.105	1.225	0.123
18	0.635	30	1.129	0.106	1.572	0.085
18	0.635	20	1.408	0.033	2.089	0.075
18	0.635	10	4.292	0.689	6.334	0.475
18	0.508	40	0.236	0.010	0.405	0.013
18	0.508	30	0.361	0.014	0.605	0.007
18	0.508	20	0.561	0.089	1.199	0.117
18	0.508	10	1.341	0.174	3.031	0.038
20	0.508	40	0.508	0.026	0.634	0.017
20	0.508	30	0.699	0.016	0.921	0.023
20	0.508	20	0.925	0.052	1.459	0.046
20	0.508	10	1.134	0.058	3.031	0.016

Analytical Results

An analytical data set of R, EI_{eff}, and F were produced for the geometries of Nitinol stylets that were manufactured for experimental validation of this analytical model. Values for d = .508mm, .635mm, .838mm, .990mm and ρ = 10mm, 20mm, 30mm, 40mm was input into the numeric solver in Maple was used to evaluate R.

Table A3.2: Numerically Calculated Values of R, EI_{eff}, F

Neutral Axis R (m)				
d,rho	10mm	20mm	30mm	40mm
.508mm	0.010297	0.020316	0.030390	0.040254
.635mm	0.010386	0.020350	0.030593	0.040317
.838mm	0.010532	0.020475	0.030504	
0.99mm	0.010645	0.020576	0.030570	0.040362
Effective Stiffness EI_{eff} (m^4)				
d,rho	10mm	20mm	30mm	40mm
.508mm	0.000123	0.000128	0.000128	0.000245
.635mm	0.000299	0.000318	0.000295	0.000599
.838mm	0.000906	0.000920	0.000948	
.990mm	0.00176	0.00177	0.00183	0.00307
Force F (N)				
d,rho	10mm	20mm	30mm	40mm
.508mm	1.56	0.409	0.180	0.195
.635mm	3.81	1.01	0.417	0.476
.838mm	11.54	2.93	1.34	
.990mm	22.37	5.65	2.59	2.44

The 40mm bend radius 508mm and .635mm diameter stylets were assumed to be completely elastic based on Figure 4.1 and the fact that Maple could not converge on a solution within the limits of integration. The 40mm bend radius .838mm stylet also could not be evaluated in Maple or Mathematica and was omitted from the Results section. Examination of the unevaluated equations shows chaotic readings ranging from -10^{20} to 10^{20} near values for R between ρ and ρ+d. One hypothesis for the failed evaluations is that the Maple and Mathematica solvers sometimes do not have the computational accuracy to solve for a variable that is both a limit of integration and in the integral. The values of F shown above were entered into Ch. 4, Equations 15-19 to solve for the friction force and unbending force applied during retraction.